


Wind speed variability over the Canary Islands, 1948–2014: focusing on trend differences at the land–ocean interface and below–above the trade-wind inversion layer

Cesar Azorin-Molina¹  · Melisa Menendez² · Tim R. McVicar^{3,4} · Adrian Acevedo² · Sergio M. Vicente-Serrano⁵ · Emilio Cuevas⁶ · Lorenzo Minola¹ · Deliang Chen¹

Received: 29 December 2016 / Accepted: 12 August 2017
© The Author(s) 2017. This article is an open access publication

Abstract This study simultaneously examines wind speed trends at the land–ocean interface, and below–above the trade-wind inversion layer in the Canary Islands and the surrounding Eastern North Atlantic Ocean: a key region for quantifying the variability of trade-winds and its response to large-scale atmospheric circulation changes. Two homogenized data sources are used: (1) observed wind speed from nine land-based stations (1981–2014), including one mountain weather station (Izaña) located above the trade-wind inversion layer; and (2) simulated wind speed from two atmospheric hindcasts over ocean (i.e., SeaWind I at 30 km for 1948–2014; and SeaWind II at 15 km for 1989–2014). The results revealed a widespread significant negative trend of trade-winds over ocean for 1948–2014, whereas

no significant trends were detected for 1989–2014. For this recent period wind speed over land and ocean displayed the same multi-decadal variability and a distinct seasonal trend pattern with a strengthening (late spring and summer; significant in May and August) and weakening (winter–spring–autumn; significant in April and September) of trade-winds. Above the inversion layer at Izaña, we found a predominance of significant positive trends, indicating a decoupled variability and opposite wind speed trends when compared to those reported in boundary layer. The analysis of the Trade Wind Index (TWI), the North Atlantic Oscillation Index (NAOI) and the Eastern Atlantic Index (EAI) demonstrated significant correlations with the wind speed variability, revealing that the correlation patterns of the three indices showed a spatio-temporal complementarity in shaping wind speed trends across the Eastern North Atlantic.

Electronic supplementary material The online version of this article (doi:10.1007/s00382-017-3861-0) contains supplementary material, which is available to authorized users.

✉ Cesar Azorin-Molina
cesar.azorin-molina@gu.se

¹ Regional Climate Group, Department of Earth Sciences, University of Gothenburg, Box 460, 405 30 Gothenburg, Sweden

² Environmental Hydraulics Institute “IH Cantabria”, Universidad de Cantabria, Santander, Spain

³ CSIRO Land and Water, Canberra, ACT, Australia

⁴ Australian Research Council Centre of Excellence for Climate System Science, University of New South Wales, Sydney, Australia

⁵ Instituto Pirenaico de Ecología, Consejo Superior de Investigaciones Científicas (IPE-CSIC), Departamento de Procesos Geoambientales y Cambio Global, Zaragoza, Spain

⁶ Izaña Atmospheric Research Center (IARC), Meteorological State Agency of Spain (AEMET), Santa Cruz de Tenerife, Spain

Keywords Wind speed · Trade-winds · Trends · Land–ocean · Inversion-layer · Atmospheric circulation · Canary Islands

1 Introduction

Global terrestrial near-surface (~10-m height) wind speed exhibited an average decline of -0.140 meters per second per decade ($\text{m s}^{-1} \text{dec}^{-1}$) over the past 50-years (McVicar et al. 2012). This “stilling” (Roderick et al. 2007) has been attributed to various causes; see Azorin-Molina et al. (2014, 2016) and McVicar et al. (2012), and the relevant references therein. The identification of the exact cause(s) is still unresolved. Global terrestrial stilling is not ubiquitous (McVicar et al. 2012), as positive trends are reported for coastal (Pinard 2007), high-latitudes (i.e., $>70^\circ$; McVicar et al. 2012; Minola et al. 2016), or the last

decade for some regions (Kim and Paik 2015; Dunn et al. 2016). Contrary to terrestrial stilling, Wentz et al. (2007) reported increased wind speed trends over oceans globally of $+0.080 \text{ m s}^{-1} \text{ dec}^{-1}$ (1987–2006) using special sensor microwave/imagers (SSM/Is), and Tokinaga and Xie (2011) found an increase in wind speed of the same magnitude, i.e. $+0.084 \text{ m s}^{-1} \text{ dec}^{-1}$ (1988–2008) adjusting ship-based anemometer readings, and of $+0.134 \text{ m s}^{-1} \text{ dec}^{-1}$ (1988–2008) using SSM/Is. Young et al. (2011) also analyzed wind speed trends over the ocean from satellite altimeter observations, reporting wind speed trends of higher magnitudes ($+0.192 \text{ m s}^{-1} \text{ dec}^{-1}$; 1991–2008).

Additionally, to date, no previous study has assessed long-term wind speed trends and variability simultaneously in the boundary layer (i.e., below the trade-wind inversion layer; hereafter TWIL) and in the lower free troposphere (i.e., above the TWIL) from land-based stations. McVicar et al. (2010) revealed that wind speeds are decreasing more rapidly at higher elevations for two inland mountainous regions, with the high-elevations sites likely still in the boundary layer (so below any TWIL). In contrast, Vautard et al. (2010) reported that upper-air (observed at an altitude of 850 hPa and above) rawinsonde wind speed data do not show a declining trend, and in some regions (e.g., Western Europe and North America) experienced wind increases during last three decades. Noting herein McVicar and Körner's (2013) definitions for 'elevation' (i.e., vertical distance between a point on the land surface and a reference point—usually mean sea level) and 'altitude' (i.e., vertical distance between an object—e.g., parcel of air—and a reference point/stratum without direct physically connection existing) are used.

Because of these discrepancies in observed near-surface wind speed trends at the land (i.e., negative trends)—ocean (i.e., positive trends) interface, and the uncertainties in trends below—above the TWIL (which is hampered by the few studies of wind speed trends in the lower free troposphere) further investigation is needed. This is especially the case if both aspects can be studied simultaneously, which has previously not been performed. The Canary Islands, surrounded by sea and with land-surface elevations exceeding 3700 m, provides the opportunity to simultaneously assess both land—ocean and below—above TWIL wind-speed trends. The subtropical Canary Island archipelago and the surrounding Eastern North Atlantic Ocean is an understudied region, and therefore this study fills the gap in the global wind speed trends compiled by McVicar et al. (2012). Additionally, this represents a key region (i.e., a 'hot-spot', as it is halfway between tropical and subtropical areas) for studying trade-wind variability associated with the subtropical high pressure belt (i.e., Azores high pressure) and the dominance of north-easterly trade-winds that blow out of the equatorward flank of this subtropical anticyclone system. Hence our

objectives are to: (1) report for the first time wind speed variability over the Canary Island and surrounding Eastern North Atlantic Ocean for 1948–2014; (2) simultaneously assess wind speed trend differences across the land—ocean interface, and below—above the TWIL; and (3) investigate the role played by changes in the large-scale atmospheric circulation on the spatio-temporal variability of wind speed, with focus on trade-winds.

2 Study area and datasets

2.1 Study area

The Canary Islands are an archipelago located between 27.6° – 29.4° N, and 13.3° – 18.2° W, in the subtropical Eastern North Atlantic region (Macaronesia) greatly affected by the Azores high pressure system and associated trade-winds (Cropper and Hanna 2014), approximately 100-km west from the African continent (Fig. 1). All seven islands are volcanic in origin with very complex steep terrain (high surface roughness). The overall average elevation is 532 m a.s.l. (standard deviation of 372.6 m), and Mount Teide (3718 m a.s.l.) on Tenerife is the maximum elevation. The islands have a subtropical climate characterized by warm air temperatures throughout the year (mild winters with a mean air temperature $>20^{\circ}\text{C}$), low precipitation ($<225 \text{ mm year}^{-1}$; east islands are desert with $<100 \text{ mm year}^{-1}$) and high sunshine ($>2800 \text{ h year}^{-1}$). Prevailing north-easterly trade-winds driven by the Azores high pressure system dominate below $\sim 1500 \text{ m a.s.l.}$ (Carrillo et al. 2016); which bring moisture, Stratocumulus fog and occult precipitation, forming subtropical dense forests on some well-exposed northern and north-easterly areas (García-Santos et al. 2004). Our study area extends out to the surrounding Atlantic Ocean (Fig. 1) to assess wind speed trends across the land—ocean interface and to account for local wind jet/shadow areas due to interisland and coastline morphology.

2.2 Land wind speed observations

Observed land wind speed data were recorded at 'first-order' meteorological stations (i.e., maintained by official weather service staff that ensured measurements to be accurately and periodically calibrated and handle with care) and supplied by the State Meteorological Agency of Spain (AEMET). All stations are airports, except for the high mountain Izaña Atmospheric Observatory, which also ensure less immediate proximal environment changes. Wind speeds were measured using two types of anemometers (specifically the anemograph universal 82a and anemometer SV5; for descriptions see Azorin-Molina et al. 2014) and assumed (in the absence of metadata) to be acquired at the standard World

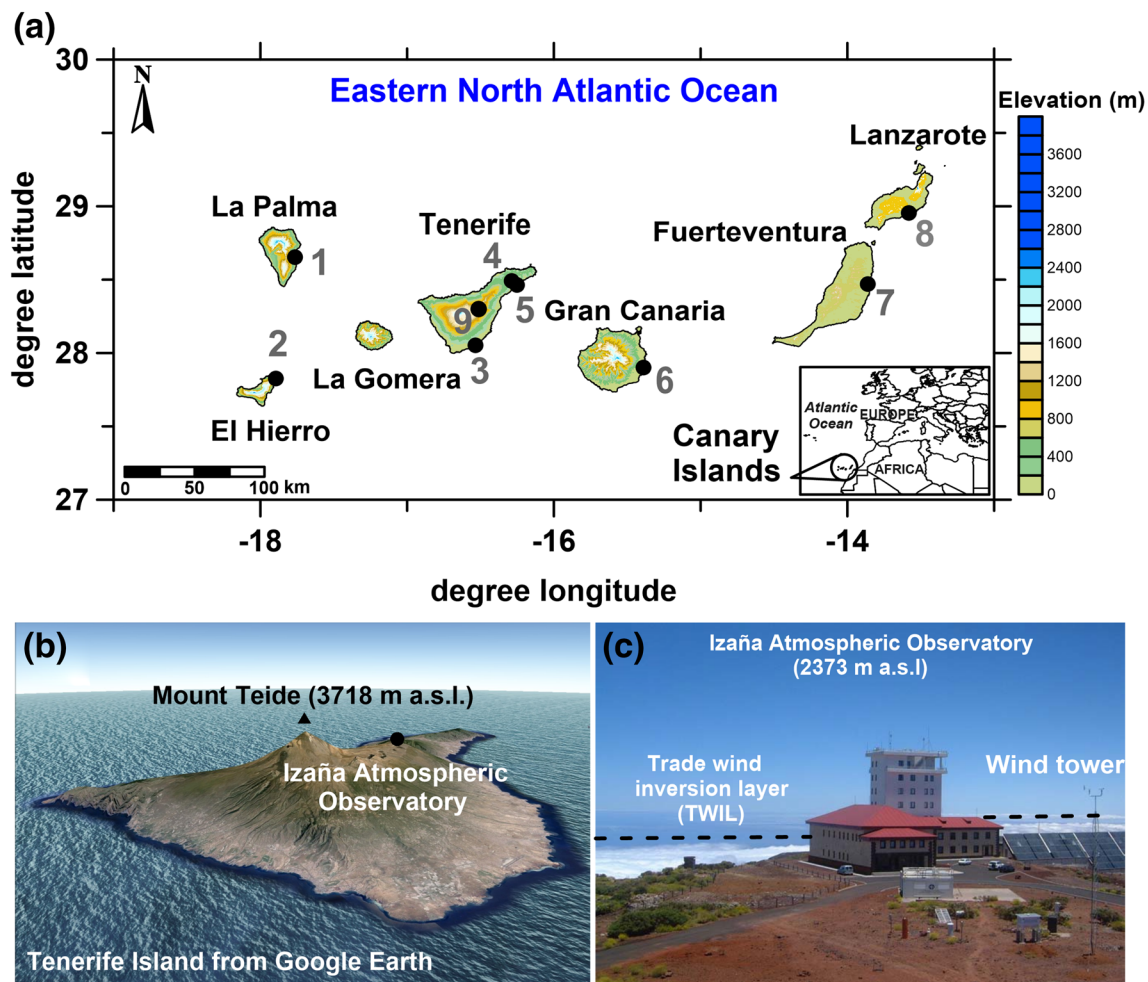


Fig. 1 **a** Terrain map of the Canary Island archipelago (totalling 7446 km²) and the surrounding subtropical Eastern North Atlantic Ocean, showing locations of nine land-based stations (black circles and numbers). **Bottom pictures b, c** illustrate the location of the Izaña Atmospheric Observatory above the trade-wind inversion layer

(TWIL) at 2373 m a.s.l. Surface areas for each island: La Palma (708.32 km²), El Hierro (268.71 km²), La Gomera (369.76 km²), Tenerife (2034 km²), Gran Canaria (1560 km²), Fuerteventura (1660 km²), and Lanzarote (845.94 km²)

Meteorological Organization (WMO) height of 10 m. Raw monthly wind speed data (in m s⁻¹) supplied by the AEMET were derived from daily mean wind speed data averaged from standard 10-min mean observations made at 0000, 0700, 1300, and 1800 UTC (i.e., a difference of 1 h for two of the WMO's standard observing times of 0600 and 1200 UTC). Monthly means were computed for days with three or more observations a day and for those months having at least 26 days observed, and if not, the whole day or month was excluded and set as missing (Azorin-Molina et al. 2014). The raw terrestrial wind speed dataset across the Canary Islands comprises nine series, with high representativeness of the archipelago. The observational land-based station network observes two key tropospheric layers, with: (1) eight low-elevation land-stations located near the coast and below the TWIL where trade-winds dominate; and (2) one mountain

weather station above a quasi-permanent marine boundary layer in the Izaña Atmospheric Observatory at 2373 m a.s.l. (<http://izana.aemet.es/index.php?lang=en>; last accessed 1 June 2017) where free-troposphere winds (almost permanent north-westerly flows above the TWIL) prevail (Cuevas et al. 2013). Therefore, wind speed within and above TWIL have been homogenized and analyzed separately.

Observed wind speed datasets were subjected to a quality control and homogenization protocol to remove systematic errors (i.e., inhomogeneities) due to multiple causes (Pryor et al. 2009) and uncertainties due to the lack of metadata. A first quality control (Aguilar et al. 2003) was conducted by AEMET which removed anomalous daily data and checked for data consistency, discarding gross errors (outliers) due to archiving, transcription, and digitalization (El Kenawy et al. 2013). For the eight stations located below TWIL we used

the recently developed relative homogeneity test HOMER (HOMogenization softwarE in R). This semi-automatic homogenization tool compares each candidate series with a number of available series without the need of creating reference series (Mestre et al. 2013); its use is supported by Venema et al. (2012). The fully automatic joint segmentation with a partly subjective pairwise comparison of HOMER ensures the detection of inhomogeneities in wind speed time series without having comprehensive station metadata describing artificial changes in the series. HOMER used all eight wind speed series to each candidate station to check for break points and selected ratios as a measure for annual comparisons. This homogenization approach was applied to each of the eight observed wind speed series, in turn, correcting the detected breaks and filling data gaps based on Eq. (8) of Mestre et al. (2013).

For the Izaña Atmospheric Observatory, because of: (1) its location above the TWIL; (2) different wind speed variability in the free troposphere; and (3) the lack of neighboring similar-environment stations, the homogenization was applied independently by using wind speed at the 700 hPa geopotential height (~3000 m a.s.l. representing the free troposphere and not affected by trade-winds; grid-point 27.5°N–17.5°W) from the NCEP/NCAR reanalysis (Kalnay et al. 1996) as reference series. Even though reanalysis datasets may also be affected by breakpoints (Sterl 2004), annual Pearson's correlation coefficient (r) of the first differences between wind speed at the Izaña Atmospheric Observatory and wind speed at the 700-hPa geopotential height is 0.7, with monthly r -values ranging from 0.9 (January) to 0.3 (June) when the strongest and weakest synoptic winds occur, respectively (Cuevas et al. 2013). These correlation coefficients are comparative to other references series used in previous homogenization studies (Azorin-Molina et al. 2014; Minola et al. 2016). We adopted a conservative approach

in homogenizing this wind speed series by only adjusting statistically significant breakpoints (at the 5% level) when the relative Alexandersson's Standard Normal Homogeneity Test (SNHT; Alexandersson 1986; using the AnClim package developed by; Stepanek 2004) detected a number of monthly inhomogeneities around the same year. For data completeness, we filled missing values by using the above-mentioned reanalyzed wind speed.

Thus, the observed wind speed dataset consists of nine homogenized series across the Canary Island archipelago (see Fig. 1), which is a reasonable number in terms of spatial data density for terrestrial stilling studies (1 station per 833 km²) compared to other studies (e.g., 1 station per 7384 km² for Spain and Portugal in Azorin-Molina et al. 2016, and 1 station per 48,125 km² for Australia in; McVicar et al. 2008). Azorin-Molina et al. (2016) concluded that few stations (i.e., ~5–10) are enough to capture the decadal variability and trends of wind speed. As the temporal coverage of these nine wind speed time series is very heterogeneous (see Table 1), with digitized data starting at different decades and suffering from a substantial lack of records prior to 1981, we reported the land near-surface wind speed dataset during the 34-year 1981–2014, and especially focused on the common 1989–2014 extent (see below).

2.3 Ocean wind speed hindcasts: SeaWind

Two ocean wind speed datasets are used here to analyze wind speed trends in the subtropical Eastern North Atlantic Ocean surrounding the Canary Islands: (1) SeaWind I, a 30-km horizontal resolution hindcast product derived from initial and boundary conditions supplied by the NCEP/NCAR reanalysis I (1948–2014); this long-term product minimizes the constraint of short (i.e., last three decades) data availability of previous studies (Wentz et al.

Table 1 Description of the land based stations across the Canary Islands archipelago (for locations see numbers in Fig. 1) and SeaWind I and II hindcast products

#	Id	Station name/# grid points	Latitude/domain (decimal°)	Longitude/domain (decimal°)	Elevation a.s.l. (m)	Location	Start date (mm/yyyy)
1	C139E	La Palma	28.63	−17.76	33	Coast	04/1970
2	C929I	El Hierro	27.82	−17.89	32	Coast	12/1973
3	C429I	Tenerife S	28.05	−16.56	64	Coast	07/1980
4	C447A	Tenerife N	28.48	−16.33	632	Inland	01/1961
5	C449C	SC Tenerife	28.46	−16.26	35	Coast	01/1943
6	C649I	Gran Canaria	27.92	−15.39	24	Coast	01/1961
7	C249I	Fuerteventura	28.44	−13.86	25	Coast	10/1969
8	C029O	Lanzarote	28.95	−13.60	14	Coast	11/1972
9	C430E	Izaña	28.31	−16.50	2373	Mountain	01/1916
–	SeaWind I	700	[26.0, 31.0N]	[12.0, 20.0W]	10	Ocean	01/1948
–	SeaWind II	2408	[26.0, 31.0N]	[12.0, 20.0W]	10	Ocean	01/1989

For SeaWind products, elevation refers to the vertical distance above the ocean surface that wind speed is simulated

2007; Tokinaga and Xie 2011; Young et al. 2011) to characterize oceanic wind speed trends; and (2) the SeaWind II dataset, a 15-km horizontal resolution hindcast product retrieved from the ERA-Interim Reanalysis (1989–2014). The Weather Research and Forecasting (WRF) model with the Advanced Research WRF dynamical solver (Skamarock et al. 2008) was employed to create the two dynamically downscaled wind products. SeaWind hindcasts were obtained from a daily re-forecast running mode and the Yonsei University (YSU) Planetary Boundary Layer (PBL) parameterization scheme after a sensitivity analysis. The analyzed regions from the SeaWind datasets are bounded by 26.0–31.0°N and 12.0–20.0°W with 700 grid points for SeaWind I and 2408 grid points for SeaWind II, covering an ocean area of 228,110 km² (excluding the archipelago). Vertically, the model comprised 42 hybrid full levels (14 additional levels were added in between the lowest eta full-levels against the standard 28-level distribution) with the top level at 50 hPa. Lastly, 10-m wind speed series were retrieved, with outputs recorded at hourly intervals, from which we derived monthly means for oceanic wind speed trend analyses. Detailed descriptions of both hindcast products including the model set-up, validation and climate characterization, are found in Menendez et al. (2014). The land wind speed observations were not used in the assimilation data procedure of the reanalyses

and therefore winds from the SeaWind datasets and the land wind speed observations are completely independent.

Because in-situ observed wind records over the ocean are generally scarce (only two buoys), we validated the SeaWind I and SeaWind II hindcast products against 10-m wind speed derived from the backscatter coefficient of a multi-mission and inter-calibrated altimeter dataset: i.e., Geosat, Topex/Poseidon, Jason-1, Envisat and Geosat Follow-On missions from 1992 to 2013. Satellite-SeaWind hindcast comparison was performed by: (1) selecting the corresponding simulated SeaWind value for each satellite observation; (2) aggregating the pairs of data to grid-boxes of $0.5 \times 0.5^\circ$; and (3) estimating the bias and correlation from the samples of each grid-box. Figure 2 shows the good agreement between wind speed altimeter observations and SeaWind wind speed hindcasts with Pearson's correlation values higher than $r = 0.8$, reaching values higher than $r = 0.9$ for SeaWind II north of the Canary Islands and lower values (about $r = 0.7$) southwest of the archipelago and closer to the African coast. Bias is lower than 1 m s^{-1} for SeaWind II with a slight underestimation bias for SeaWind I, particularly over the northwest region. Moreover, the SeaWind hindcast products show a better performance in reproducing wind vectors in comparison with its driving reanalyses (see Sect. 4.1 below).

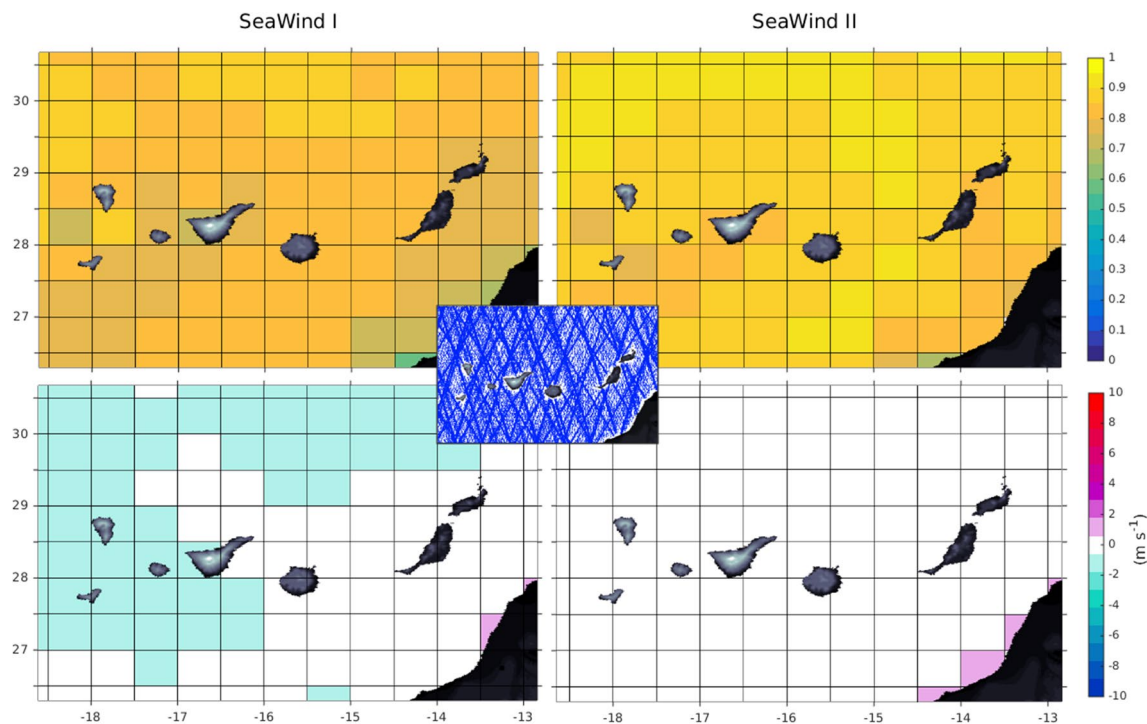


Fig. 2 Spatial distribution of Pearson correlation r values (*top row*) and bias (*bottom row*) for the intercomparison between wind altimeter satellite observations and the hindcast ocean wind speed data, Sea-

Wind I and SeaWind II. Tracks of the satellite data used (1992–2013) are displayed in the *middle* of the figure

2.4 Atmospheric circulation indices

Three atmospheric circulation indices were chosen for a complete description of the interplay between them in modulating climate variability of near-surface wind speed. Firstly, we used Cropper and Hanna's (2014) trade wind (TW), a more regional circulation mode recently developed for the Macaronesia region. The TW Index (TWI) is retrieved as the station-derived normalized pressure between the Azores and Cape Verde and was directly supplied by Cropper and Hanna (2014). Secondly, we analyzed the North Atlantic Oscillation (NAO; Jones et al. 1997) climate mode, with the station-based NAO index (NAOI) defined as the normalized sea level pressure between Gibraltar and Reykjavik as obtained from the Climate Research Unit (available online at <https://crudata.uea.ac.uk/cru/data/nao/>; last accessed 1 June 2017). Thirdly, and finally, we used the East Atlantic (EA) as the second leading climate mode of low-frequency variability covering the meridional positions of the centers of action in the North Atlantic, with the EA index (EAI) as a north–south dipole of anomaly center spanning the North Atlantic from east to west, similar to that shown in Barnston and Livezey (1987). EAI was retrieved from the NOAA-NCEP at <http://www.cpc.ncep.noaa.gov/data/tel-edoc/ea.shtml> (last accessed 1 June 2017). The transects for these three atmospheric circulation indices in relation to the large-scale pressure systems (i.e., the Azores high, and the Icelandic and African lows) are shown in the Supplementary Figure S1, denoting the complementarity in describing distinct atmospheric dynamics of each one because the different influence of these three major pressure systems. The combination of the three climate modes is crucial for better attributing wind speed variability to changes in large-scale atmospheric circulation at different time-scales.

3 Statistical methods

Station and hindcast (i.e., offshore grid-cells for both SeaWind datasets) time series were firstly expressed as wind speed anomalies (in m s^{-1}) from the 1981–2010 mean; except for the common 1989–2014 extent (see below) when anomalies were computed for this 26-year period. Regional series were also computed by averaging wind speed anomalies for the eight land-based stations (i.e., except for the Izaña Atmospheric Observatory which was analyzed separately) and all grid points in the hindcast domain. Then, a linear regression analysis was applied between the series of time (independent variable) and the wind speed anomaly series (dependent variable) to retrieve the sign and magnitude of the wind speed trend. The slope of the linear regression model represents the wind speed

trend in meters per second per decade ($\text{m s}^{-1} \text{dec}^{-1}$). Multi-decadal variability of wind speed is illustrated by plotting a 15-year Gaussian low-pass filter.

To measure the degree to which a trend is consistently increasing or decreasing, we first accounted for the autocorrelation function of wind speed anomaly series (von Storch 1995) since significant autocorrelations may increase the probability of significant trends. A 1-month lag autocorrelation coefficient was applied on the series and there was no significant serial correlation beyond lag 0 at the $p < 0.05$ significant level; therefore, the commonly used pre-whitening procedure for removing autocorrelation was not applied. We then used the nonparametric correlation coefficient of Mann–Kendall's tau-b (Kendall and Gibbons 1990) to measure the statistical significance of annual, seasonal and monthly linear trends, as the tau-b test is more robust than parametric methods as it does not require normality of the data series (Lanzante 1996). Moreover, the statistical significance of the trends is reported at three p level thresholds (significant at $p < 0.05$; significant at $p < 0.10$; and not significant at $p > 10$) following McVicar et al. (2010) and Azorin-Molina et al. (2014, 2016) to evaluate the uncertainty of wind speed estimated trends. Field significance of the detected significant trends at the 95% confidence level was evaluated by applying the Livezey and Chen (1983) and Wilks (2006) method to detect whether station or grid series with significant trends occurred by chance (Dadaser-Celik and Cengiz 2014). To quantify the statistical significance of trend differences between datasets the Clogg et al. (1995) test was used. Pearson's correlation coefficient (r) was employed to measure the relationship between the atmospheric circulation indices and the observed and dynamically downscaled wind speed anomalies. We primarily assessed annual and seasonal [defined as winter (DJF), spring (MAM), summer (JJA), autumn (SON)] trends, with some monthly analyses also presented to better discern interesting features of the intra-annual variability of wind speed trends.

We present trends for two time-periods: (1) 1948–2014 (i.e., 67 years) for SeaWind I; and (2) 1989–2014 (i.e., 26 years) for all observed and simulated datasets. The motivation to report wind speed variability over these two time spans lies in: (1) covering a historical long-time period never before explored for SeaWind I during 1948–2014; and (2) adding the novelty of simultaneously assessing wind speed trends at the land–ocean interface and below–above the TWIL for the common 1989–2014 period. For the land-observations, we also reported as complementary information variability and trends for 1981–2014. Figure 3 summarizes the time covered by each dataset over the 1948–2014 period.

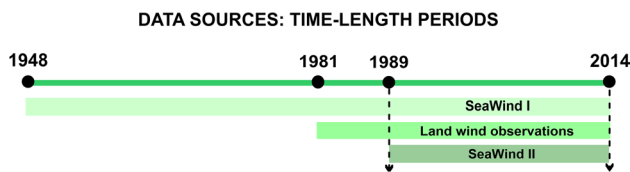


Fig. 3 Diagram summarizing the time-length periods covered by the SeaWind I (1948–2014), land wind observations (1981–2014) and SeaWind II (1989–2014). The latter time span (delimited by *dashed lines*) is the common period to compare wind speed trends from the three datasets at the land–ocean interface and below–above the TWIL

4 Results

4.1 Wind climatology

Figure 4 compares the annual wind climatology for SeaWind I and SeaWind II against their driving NCEP/NCAR and ERA-Interim reanalyses, respectively. Both SeaWind products reproduce 10-m mean wind speed and direction vectors with a much higher horizontal resolution than the reanalyses, capturing with detail the spatial features of north-easterly trade-winds driven by the Azores high pressure system

over the Canary Islands and the surrounding Eastern North Atlantic Ocean. Among the four maps shown in Fig. 4, the SeaWind II dataset better shows the characteristic features of wind because its higher horizontal resolution (15-km horizontal grid spacing); e.g., note the strengthening of wind speed occurred offshore due to the channelling effect between the islands which is missed by the reanalyses and poorly reproduced by the SeaWind I hindcast.

Therefore, Fig. 5 only looks at seasonal wind climatology for the SeaWind II product, also including mean wind statistics from land observations; Supplementary Figure S2 shows monthly wind climatologies. Annually (Fig. 4), mean wind speed ranges from ~ 6 to 9 m s^{-1} over the ocean, whereas over land (eight stations below the TWIL) complex surface roughness among other factors weakens wind speed to $\sim 4\text{--}5 \text{ m s}^{-1}$. Seasonally (Fig. 5), north-easterly trade-winds are higher in summer exceeding $>10 \text{ m s}^{-1}$ over oceans ($\sim 5\text{--}8 \text{ m s}^{-1}$ over land), and weaker in winter–autumn oscillating around $\sim 5\text{--}8 \text{ m s}^{-1}$ for ocean ($3\text{--}5 \text{ m s}^{-1}$ for land). In contrast, the Izaña Atmospheric Observatory shows an opposite (stronger and weaker winds in winter and summer, respectively) and statistically significant negative correlations when compared to all other land stations ($r \sim -0.5$ to

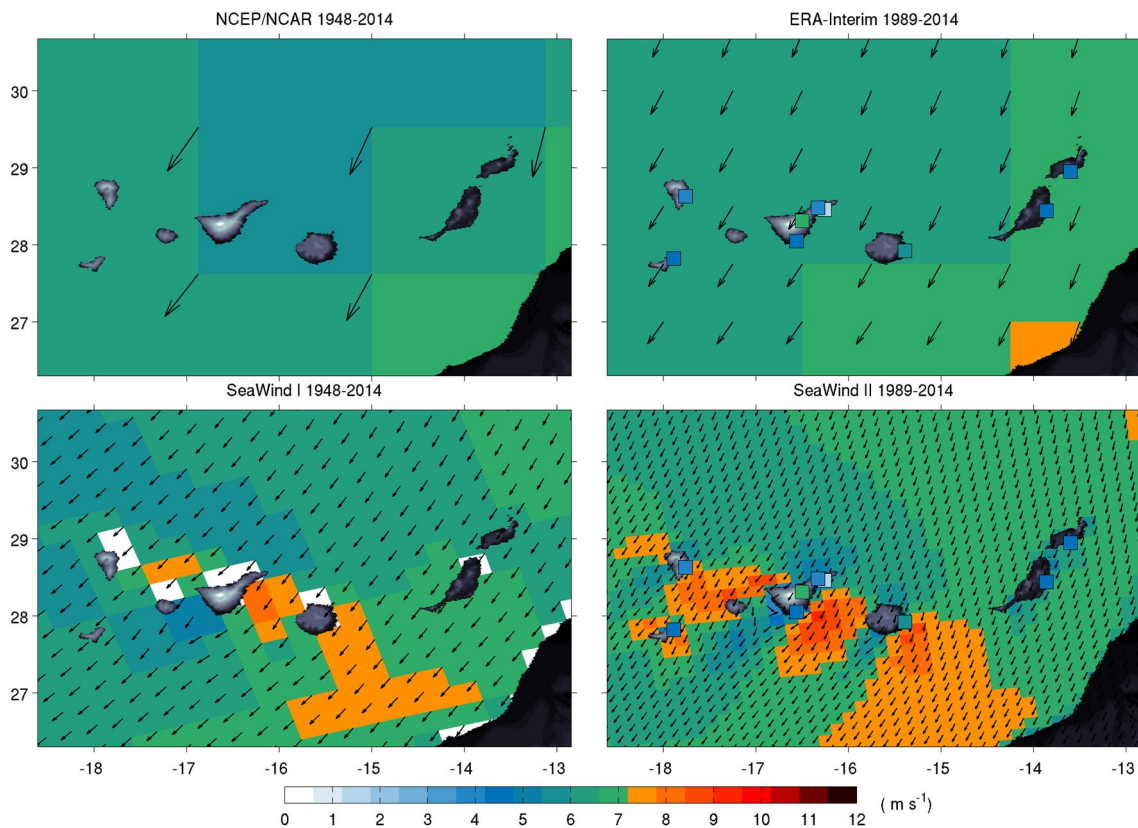


Fig. 4 Annual mean wind speed and direction vectors over the ocean from the global NCEP/NCAR and ERA-Interim reanalyses on the *top row*, and their respective SeaWind downscaled products on the *bot-*

tom row. Mean wind speed for the nine-land based stations is shown with *squares* for 1989–2014

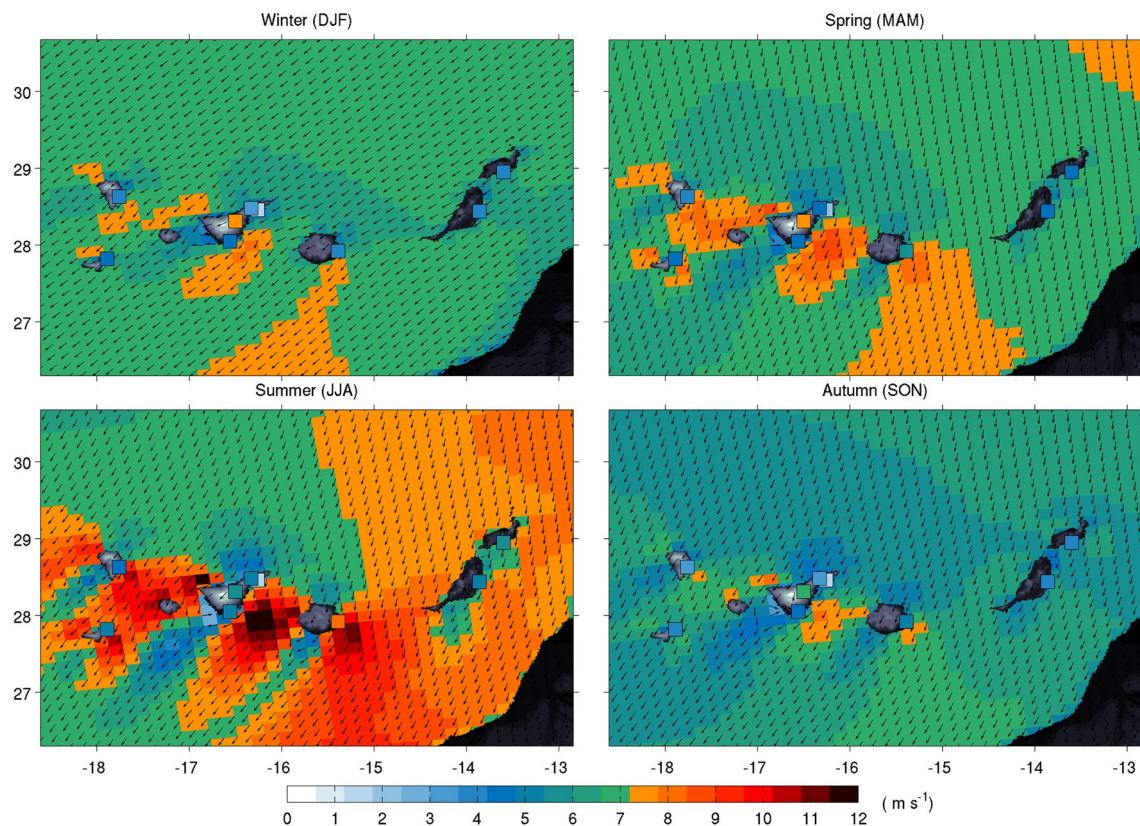


Fig. 5 Seasonal mean wind speed and direction vectors for the highest horizontal resolution (15 km) SeaWind II product and the nine-land based stations—shown as *squares*—for 1989–2014

−0.8; $p < 0.05$) because of its location above the TWIL being representative of the subtropical Eastern North Atlantic free troposphere. SeaWind II has the ability of simulating the role of complex orography of the Canary Island archipelago on oceanic wind fields, with both Figs. 4 and 5 (and the Supplementary Figure S2) showing a clear strengthening of wind speed between the islands due to the acceleration of the flow (“venturi effect”; e.g., between Tenerife and Gran Canaria), and a weakening of wind speed on the leeward sides (i.e., south-western oceanic regions proximal to the islands) against the prevailing north-easterly trade-winds.

4.2 Trends and multi-decadal variability of wind speed

Table 2 reports annual, seasonal and monthly wind speed trends for the various products using different time lengths, with 1989–2014 being the common period for comparison purposes. For SeaWind I (1948–2014) oceanic wind speed significantly declined annually and seasonally, except for winter when the weak declining trend is not significant. That is, major and significant declines occurred from April till October. This widespread slowdown of oceanic wind speed was not observed over land when analysing the much shorter 1981–2014 extent, with the eight stations below the

TWIL revealing a slight but not significant annual, spring and summer increases, and winter and autumn declines. On a monthly basis we detected major and statistically significant declines in October, and more interestingly, a strengthening of trade-winds in May–June (also November). Above the TWIL at Izaña, wind speed trends showed an almost opposite pattern for the same 1981–2014 extent, exhibiting a statistically significant increase annually, being major significance in autumn and winter, and a lesser increase in spring and summer. This nearly opposite trend behaviour is noticeable at monthly basis, e.g. the most extreme negative trends of wind speed in Izaña occurred in May, when major positive trends were reported for the eight land stations below the TWIL, whereas most positive trends in Izaña occurred in September–October when the major and significant negative trends from the eight-station observations occurred below the TWIL.

This finding of opposite wind speed trend behaviour below and above the TWIL is clearly discernible when comparing the wind speed trends for all land and ocean datasets during the common 1989–2014 period. Both SeaWind I and SeaWind II exhibited almost identical wind speed trends, but with declines which are only statistically significant for SeaWind I annually and in spring and autumn, and for SeaWind

Table 2 Annual, seasonal and monthly wind speed trends for SeaWind I, SeaWind II, eight low-elevation land-stations and Izaña for the different time periods (on the left), and for the common 1989–2014 extent (on the right)

Periods	Different time extents			Common 1989–2014 extent			
	SeaWind I 1948–2014	Observed 1981–2014	Izaña 1981–2014	SeaWind I	SeaWind II	Observed	Izaña
Annual	(−0.064)	+0.023	(+0.316)	−0.077	−0.008	+0.032	(+0.587)
Winter (DJF)	−0.016	−0.020	+0.366	−0.086	−0.047	+0.019	(+0.784)
Spring (MAM)	(−0.058)	+0.042	+0.215	−0.153	−0.050	+0.007	(+0.408)
Summer (JJA)	(−0.100)	+0.067	+0.188	+0.038	+0.133	+0.096	(+0.430)
Autumn (SON)	(−0.082)	−0.014	(+0.505)	(−0.144)	−0.114	−0.016	(+0.782)
January	−0.033	−0.105	+0.227	−0.197	−0.160	−0.013	(+1.068)
February	+0.014	+0.072	+0.488	−0.064	+0.009	+0.046	(+1.015)
March	+0.011	−0.060	+0.501	−0.210	−0.134	−0.072	+0.471
April	−0.090	+0.040	+0.363	(−0.499)	−0.394	−0.209	(+0.987)
May	−0.094	+0.145	−0.218	+0.249	+0.377	(+0.303)	−0.234
June	−0.068	+0.125	(+0.430)	+0.041	+0.143	+0.083	(+0.788)
July	−0.094	+0.057	+0.239	−0.011	+0.052	+0.055	(+0.467)
August	(−0.138)	+0.021	−0.105	+0.082	+0.204	+0.149	+0.035
September	(−0.164)	−0.082	(+0.780)	−0.339	−0.344	−0.200	(+0.800)
October	(−0.068)	−0.089	(+0.330)	−0.089	−0.075	−0.002	(+0.498)
November	−0.014	+0.129	+0.406	−0.005	+0.076	+0.152	(+1.046)
December	−0.028	+0.018	+0.348	+0.116	+0.146	+0.089	+0.106

Units are $\text{m s}^{-1} \text{dec}^{-1}$ Statistically significant trends were defined as those $p < 0.10$ (in bold) and $p < 0.05$ (in bold and in parenthesis)

II in autumn. A major finding when comparing trends across the land–ocean interface is that the land observations below the TWIL essentially resembled the reported trends over ocean with a correlation coefficient of $r > 0.9$ ($p < 0.05$) as shown in the Supplementary Figure S3. The most interesting feature in the monthly variability of wind speed trends shown in Figure S3 (and Table 2) is the statistically significant decreases detected in April, and significant increase in May for land and ocean datasets below the TWIL. When looking above the TWIL, Izaña showed strong and statistically significant increases annually and for all seasons and months. The only exception is the negative trend found in May, which contrasts with the positive tendency reported for this month over land and ocean below the TWIL. The above mentioned opposite trend pattern below and above the TWIL is statistically significant ($p < 0.05$) and the reported wind speed trends at Izaña are negatively correlated with SeaWind I and SeaWind II ($r = -0.66$) and 8-land series ($r = -0.57$).

Figure 6 displays the annual and seasonal wind speed anomalies for SeaWind I, SeaWind II, and the land observations below (eight stations) and above (Izaña) the TWIL; Supplementary Figure S4 shows monthly plots. The major feature is the strong agreement between land and ocean near-surface wind speed anomalies with significant ($p < 0.05$) correlation coefficients ranging between 0.7 and 0.9 for all time scales. This supports the quality and

homogeneity of both hindcast over the ocean and the wind speed observations over land below the TWIL. In contrast, the correlation coefficients for Izaña with respect to the hindcast and observed series are weak and mostly negative, particularly in spring (March and April; $r \sim -0.4$) and autumn (September; $r \sim -0.6$). As shown by the 15-year Gaussian low-pass filter, annual long-term (1948–2014) variability of wind speed in the subtropical Eastern North Atlantic Ocean showed four general phases: (1) an increase from 1948 to 1960; (2) a decrease from 1960 to 1990; (3) a slow recovery from 1990 to 1999; and (4) a steady decline since the 2000s. This general pattern shown by SeaWind I, and replicated for the periods of overlap in the SeaWind II and the observed 8-station series (which both start later than SeaWind I—Fig. 3) is not displayed at the higher elevation Izaña station, where wind speed first declined from 1981 till the early 1990s, and abruptly increased since them. Seasonally (and monthly), these identified phases and discrepancies below and above the TWIL (i.e., in trade-wind layer and the free troposphere, respectively) are well defined, being particularly evident by the opposite tendencies with declines below the TWIL and increases at Izaña in spring (e.g., April) and autumn (e.g., September), or increases below the TWIL and declines at Izaña in spring (e.g., May) during the last two–three decades.

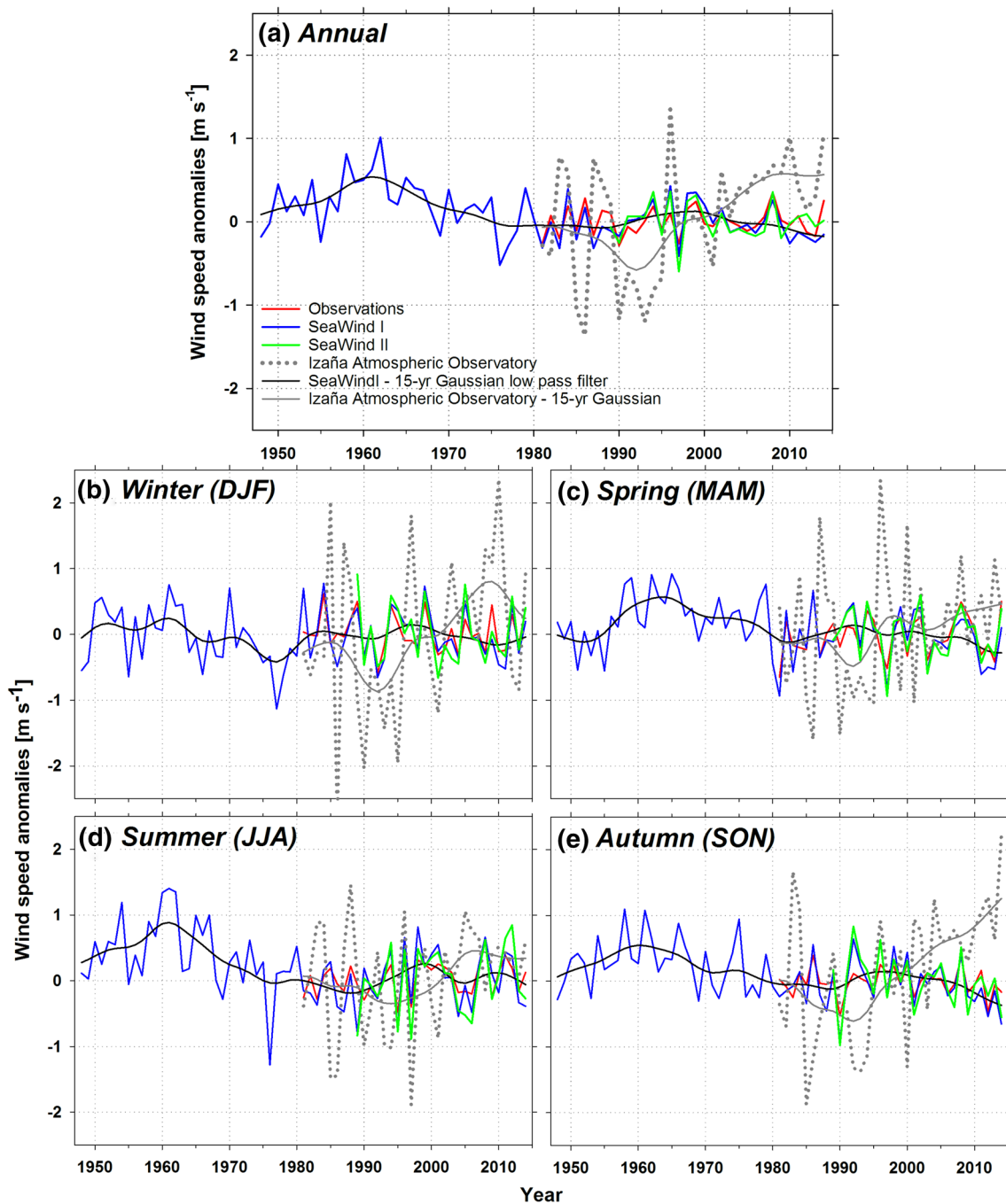


Fig. 6 Mean annual (a) and seasonal (b–e) wind speed anomalies (m s^{-1}) series SeaWind I (1948–2014), SeaWind II (1989–2014), eight low-elevation land-stations and Izaña (1981–2014). The 15-year Gaussian low-pass filter is shown for SeaWind I and Izaña. The

series are expressed as anomalies from the 1981–2010 mean, except for SeaWind II which is from the 1989–2014 mean. The legend in a applies to all other sub-parts

4.3 Spatial distribution of wind speed trends

Figures 7 (annual and seasonal) and 8 (monthly) report the spatial distribution of the sign, magnitude and statistical significance of oceanic wind speed trends for SeaWind (1948–2014); Table S1 summarizes relative frequency

statistics of both figures. The major finding of the multi-decadal variability of wind speed is the noticeable dominance of declining trends at all time-scales, being statistically significant for most grid-cells annually and in spring, summer and autumn (i.e., from April till October). The only exception of this declining tendency is winter and between

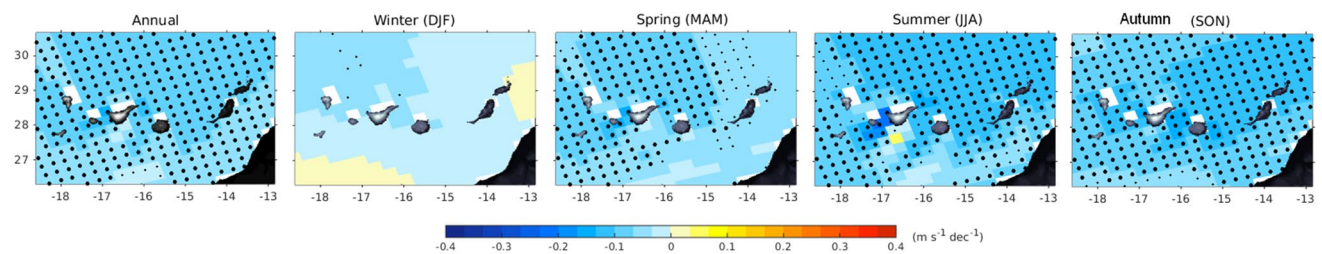


Fig. 7 Annual and seasonal spatial distribution of the sign, magnitude and statistical significance of wind speed trends for SeaWind I (1948–2014). The dots located in the centre of the grid-cells show

the statistical significance of the trends at $p < 0.05$ (large dots) and $p < 0.10$ (small dots)

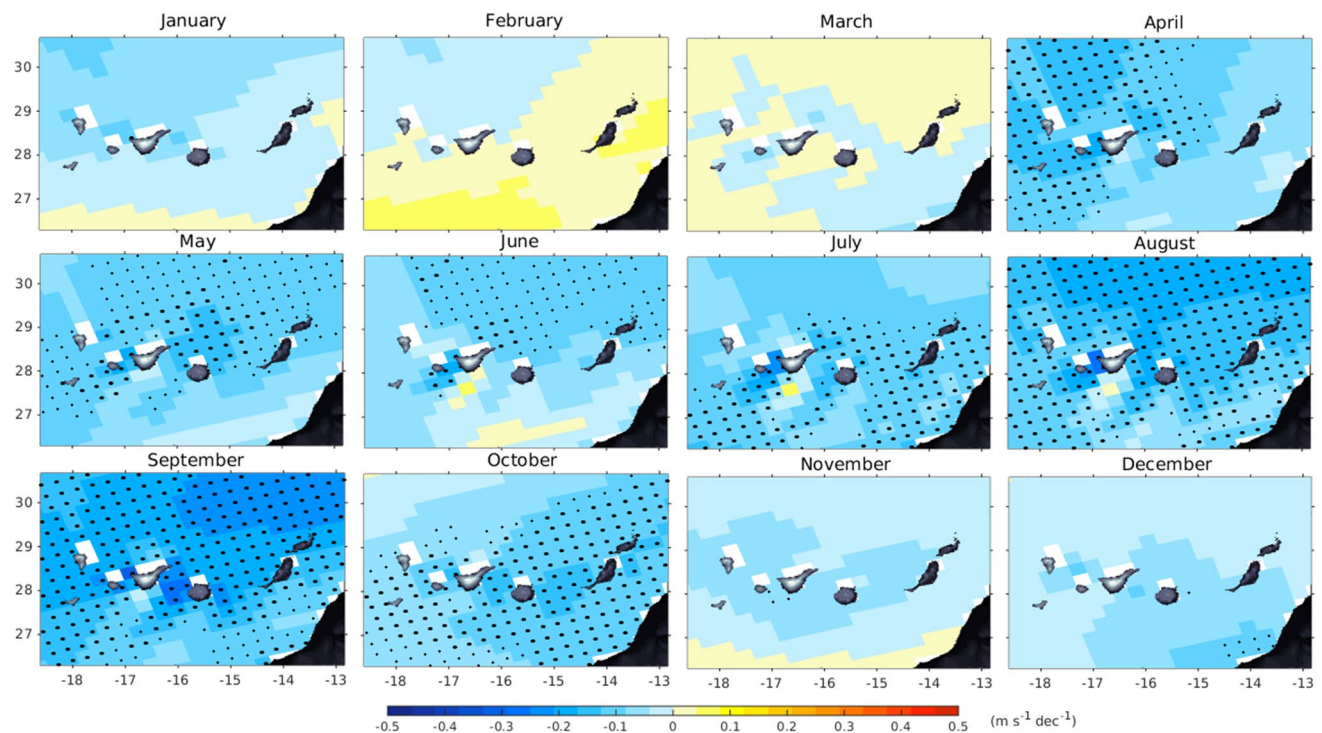


Fig. 8 As in Fig. 7 yet for monthly wind speed trends of SeaWind I for 1948–2014

November and March, when declining (or even positive in February–March) but not significant trends dominated.

Most interestingly is to compare annual and seasonal (Fig. 9) and monthly (Fig. 10) differences between SeaWind I, SeaWind II and observations at the interfaces of land–ocean and below–above the TWIL for the common 1989–2014 extent; Table 3 summarizes relative frequency statistics. Annually (Fig. 9), SeaWind I and SeaWind II showed a dominance of grid-cells reporting declining trends; the majority are significant for SeaWind I. For both hindcast products, more negative and significant wind speed trends are located in the leeward side of each island (i.e., south-western) against the prevailing north-easterly trade-winds due to the complex orography of the Canary

Islands, especially Tenerife, Gran Canaria and La Palma. This predominance of wind speed declines over ocean is not observed at the land stations annually, where half of the stations below the TWIL had opposite increasing trends. It is noticeable the differences observed on Tenerife island where all three stations below the TWIL reported negative trends whereas Izaña (located above the TWIL in the free troposphere) had a statistically significant positive trend.

Seasonally (Fig. 9), a distinct pattern with a dominance of grid-cells showing negative trends for winter, spring and autumn is found, with more declining wind speed trends being statistically significant for the latter season. A major finding when compared to the 1948–2014 extent shown in Fig. 8, is the recent and widespread increase of

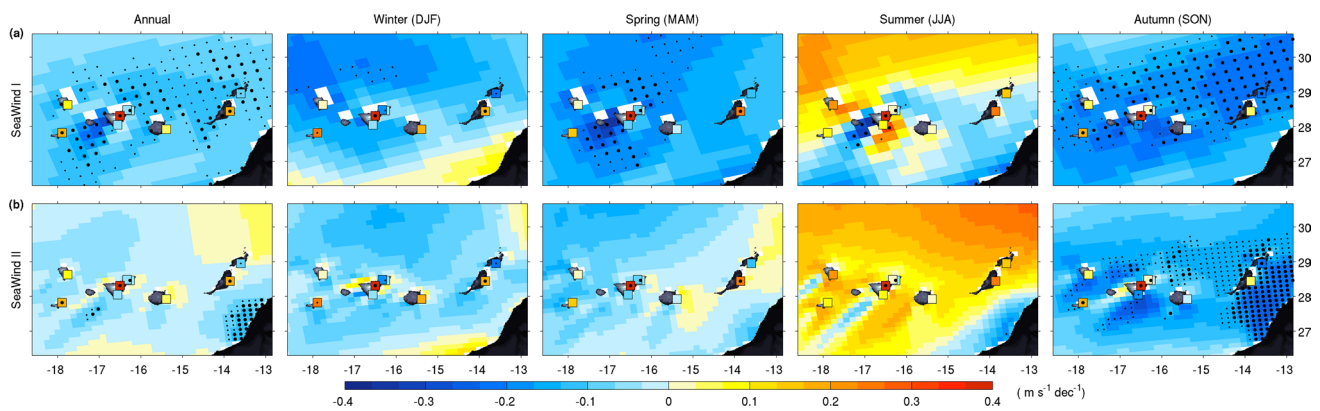


Fig. 9 Annual and seasonal spatial distribution of the sign, magnitude and statistical significance of wind speed trends for **a** SeaWind I (top row), and **b** SeaWind II (bottom row) and land-based observa-

tions for 1989–2014. The *dots located in the centre of the grid-cells* and *squares* (for observations) show the statistical significance of the trends at $p < 0.05$ (large dots) and $p < 0.10$ (small dots)

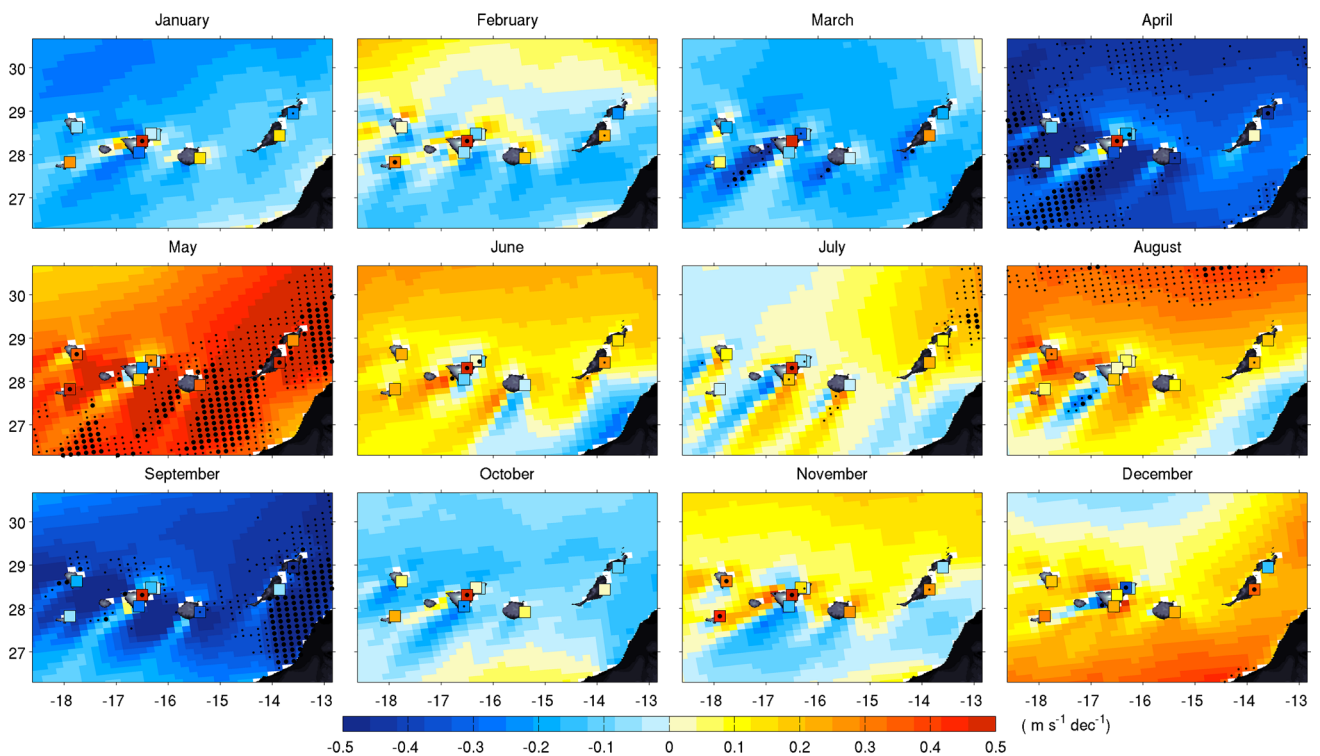


Fig. 10 Monthly spatial distribution of the sign, magnitude and statistical significance of wind speed trends for SeaWind II and land-based observations during the 1989–2014 extent. The *dots located*

in the centre of the grid-cells show the statistical significance of the trends at $p < 0.05$ (large dots) and $p < 0.10$ (small dots)

wind speed found in summer for both SeaWind I and SeaWind II. Despite being not significant, the magnitude of these positive trends is much stronger for the ocean north of the Canary archipelago and between the islands due to the abovementioned “venturi effect” (e.g., between Tenerife and Gran Canaria). Moreover, the influence of complex orography on wind trends is markedly distinguishable in summer because the dominance of increasing trends is

truncated by negative wind speed trend plumes for the south-westerly leeward sides against the north-easterly trade-winds in e.g., Tenerife, La Palma and along the shoreline of the African continent (see Fig. 9). For the land observations, an almost equal number of stations report increases and decreases in winter, spring and autumn, which contrasts the overall negative pattern encountered over ocean surfaces. The exception is summer, when eight

Table 3 Relative frequency of stations and grid-cells showing significant (at $p < 0.05$ and $p < 0.10$) and non-significant (at $p > 0.10$) negative and positive wind speed trends annually and seasonally for 1989–2014 for: (a) ocean SeaWind I (700 grid-cells), (b) ocean SeaWind II (2408 grid-cells), and (c) land observed (nine stations)

Periods	Negative	Negative sig., $p < 0.05$	Negative sig., $p < 0.10$	Negative non sig., $p > 0.10$	Positive	Positive sig., $p < 0.05$	Positive sig., $p < 0.10$	Positive non sig., $p > 0.10$
(a) Ocean SeaWind I								
Annual	98.0	18.1	42.7	57.3	2.0	0.0	0.0	100.0
Winter (DJF)	80.8	0.0	2.7	97.3	19.2	0.0	0.0	100.0
Spring (MAM)	100.0	6.8	22.4	77.6	0.0	0.0	0.0	0.0
Summer (JJA)	39.9	22.1	28.4	71.6	60.1	0.3	0.6	99.4
Autumn (SON)	98.2	27.2	43.0	57.0	1.8	0.0	0.0	100.0
(b) Ocean SeaWind II								
Annual	66.1	2.4	4.4	95.6	33.9	0.0	0.0	100.0
Winter (DJF)	85.0	0.0	0.0	100.0	15.0	0.0	0.0	100.0
Spring (MAM)	85.5	0.0	0.1	99.9	14.5	0.0	0.0	100.0
Summer (JJA)	9.5	0.0	0.6	99.4	90.5	0.0	0.2	99.8
Autumn (SON)	98.4	9.9	22.7	77.3	1.6	0.0	0.0	100.0
(c) Land observed								
Annual	44.4	50.0	50.0	50.0	55.6	60.0	60.0	40.0
Winter (DJF)	44.4	25.0	75.0	25.0	55.6	40.0	60.0	40.0
Spring (MAM)	55.6	20.0	20.0	80.0	44.4	50.0	75.0	25.0
Summer (JJA)	11.1	100.0	100.0	0.0	88.9	12.5	12.5	87.5
Autumn (SON)	44.4	50.0	75.0	25.0	55.6	40.0	40.0	60.0

For the three p -level thresholds, relative frequencies are calculated with respect to the total number of stations showing negative or positive tendencies. Spatial distributions are shown in Fig. 6

of nine stations also reported increased but not significant wind speed trends in close agreement with the hindcast positive trends over the ocean.

The spatial variability of monthly oceanic wind speed trends from SeaWind II over 1989–2014 (Fig. 10) demonstrated four distinct phases throughout the year: (1) decreases between January and April; (2) increases between May and August; (3) decreases in September and October; and (4) a predominance of increases in November and December. During the declining phase found in (1), wind speed showed the strongest and statistically significant downward trend in April. This declining trend pattern was broken in (2) with a sudden and significant strengthening of wind speed during the spring–summer period, particularly in May, whereas in phase (3) negative trends (significant in September) dominated across the entire ocean domain. Lastly, in (4) mostly positive with some few negative but not significant trends occurred in November and December. Looking at these monthly trends over land, the sign and magnitude of terrestrial wind speed trends is roughly in agreement with those four phases reported over the ocean as shown in Table 3 and Table S2, again with the exception of the mainly opposite behaviour found in Izaña above the TWIL.

4.4 Influence of atmospheric circulation on wind speed variability

The analysis of the series of the atmospheric circulation TWI, NAOI and EAI shows significant correlations in explaining the variability of wind speed over land and ocean, revealing that the correlation patterns of these three indices show a spatial and temporal complementarity in shaping wind speed trends across the Eastern North Atlantic region. Even though annual correlation values (Fig. 11; Table 4) mask key seasonal wind speed responses to changes in atmospheric dynamics and therefore are mainly weak and non-statistically significant for large areas, some complementarity features of the impact of these indices can be retrieved. To summarize: (1) the regional TWI exerted a widespread positive and significant relationship, also highlighting its positive influence on wind speed variability above the TWIL in Izaña; (2) the NAOI drove fluctuations of wind speed with a positive sign over the southern half part of the studied land–ocean domain with the exception of a strong negative correlation with Izaña; and (3) the EAI displayed a contrary negative and significant relationship over the northern half region with an opposite positive relationship in Izaña. Therefore, these overall annual correlation maps, some of them displaying negligible relationships,

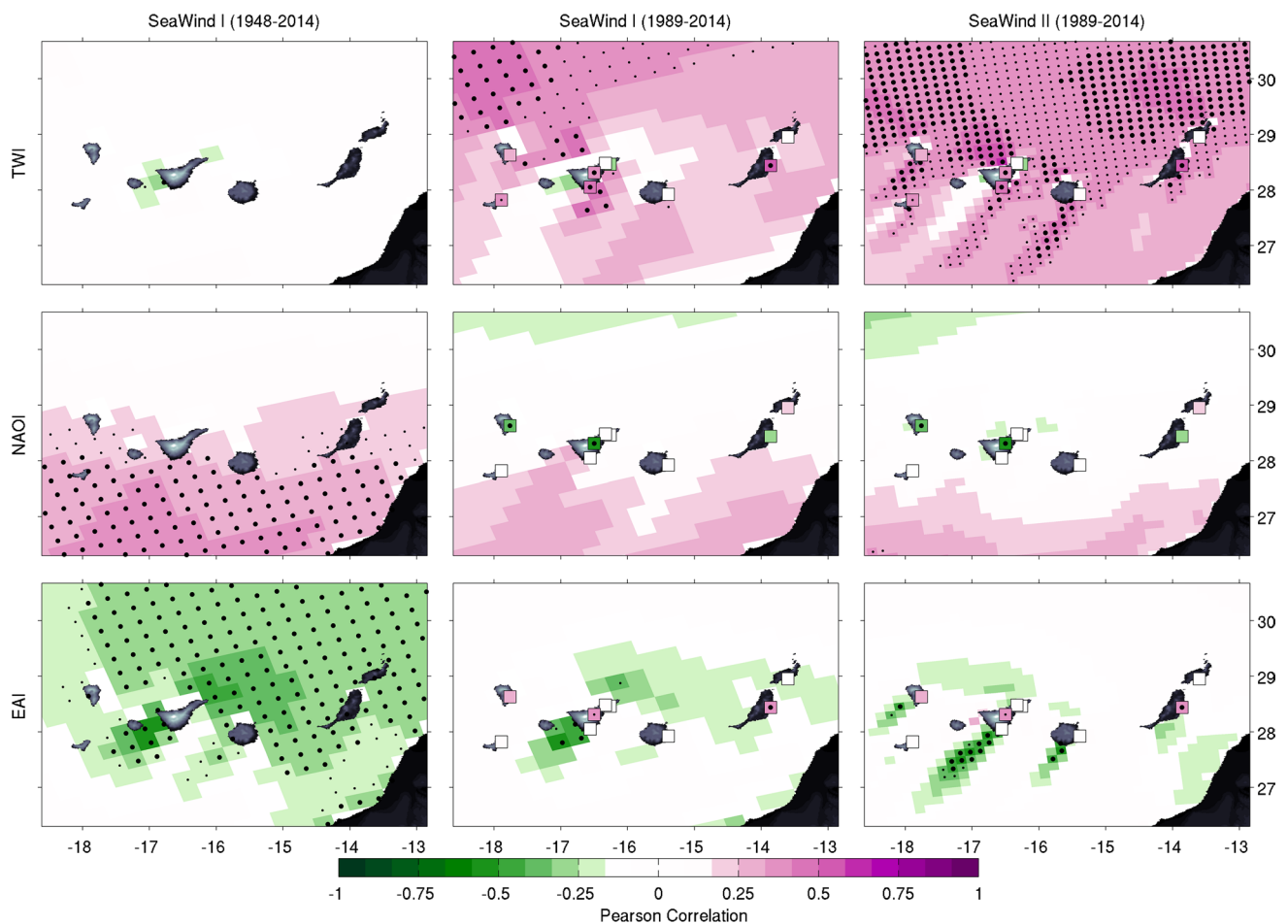


Fig. 11 Annual Pearson's correlation coefficients between wind speed anomalies and the TWI, NAOI and EAI for SeaWind I (1948–2014 and 1989–2014), SeaWind II (1989–2014), and nine land-based observations (for 1989–2014 only). The dots located in the centre of

the grid-cells and squares (for observations) show the statistical significance of the trends at $p < 0.05$ (large dots) and $p < 0.10$ (small dots)

generally indicate that the response of wind speed variability is better explained by the combination of the three circulation indices, which is confirmed in the seasonal maps shown below.

In Fig. 12 the TW positively influenced much of wind speed variability for SeaWind I mainly in winter, and secondarily in summer (much over the south-western region) for 1948–2014, reinforcing this widespread positive and significant correlation of the TWI across the ocean for all seasons (particularly in spring, summer and autumn) during the common 1989–2014 extent. Above the TWIL, the response of wind speed variability to the TWI is only positive and statistically significant in summer. Looking at the long-term tendency of atmospheric circulation indices can help to partially explain the reported trends. For 1948–2014, the TWI has become much positive for all seasons (Table 5), meaning a strengthening of trade-winds. However, wind speed declined for the historical period which might explain the weak relationship shown in Fig. 12. For the recent

1989–2014 period, the TWI has tended to be more positive particularly in summer, which likely explains the strengthening of trade-winds for land and ocean during this season, whereas the no-trend of the TWI particularly in winter and spring might explain the weakening of wind speed in both seasons.

The influence of the main synoptic mode of atmospheric circulation and climate variability in the Atlantic Ocean, i.e., the NAO, is also noticeable across the subtropical Canary Island archipelago. The response of wind speed variability to the NAOI is most remarkable when analysing seasonal correlation maps (Fig. 13), displaying a widespread and statistically significant positive relationship for winter, spring and autumn over 1948–2014. For the common 1989–2014 extent, these significant positive correlations are mainly observed in winter and autumn over ocean (non-significant for most land stations) and basically over the southern half of the region, highlighting the opposite negative and statistically significant

Table 4 Annual and seasonal Pearson's correlation coefficients between wind speed anomalies (in m s^{-1}) and the (a) TWI, (b) NAOI and (c) EAI for SeaWind I (1948–2014 and 1989–2014), SeaWind II (1989–2014), eight low-elevation land-stations (1989–2014) and Izaña (1989–2014), with $p < 0.05$ (in bold and in parenthesis) and $p < 0.10$ (in bold)

Source/period	SeaWind I/1948–2014	SeaWind I/1989–2014	SeaWind II/1989–2014	Observations/1989–2014	Izaña/1989–2014
(a) TWI					
Annual	0.008	0.321	(0.389)	0.366	(0.396)
Winter (DJF)	(0.411)	(0.418)	(0.448)	0.249	−0.075
Spring (MAM)	0.079	0.359	(0.448)	(0.469)	0.005
Summer (JJA)	0.197	0.368	0.350	(0.492)	0.386
Autumn (SON)	0.158	0.304	0.370	0.357	0.073
(b) NAOI					
Annual	0.169	0.024	−0.029	−0.144	(−0.550)
Winter (DJF)	(0.296)	(0.389)	0.346	0.320	(−0.596)
Spring (MAM)	(0.316)	0.229	0.162	0.219	(−0.570)
Summer (JJA)	0.123	−0.056	−0.113	−0.253	−0.280
Autumn (SON)	(0.272)	0.332	0.283	0.318	−0.135
(c) EAI					
Annual	−0.236	−0.051	−0.024	0.166	0.370
Winter (DJF)	(−0.273)	−0.221	−0.299	−0.111	−0.087
Spring (MAM)	−0.014	0.052	0.043	0.102	−0.006
Summer (JJA)	0.233	(0.494)	(0.593)	(0.550)	0.163
Autumn (SON)	−0.209	−0.109	−0.080	−0.074	0.261

Spatial distributions of grid-cells and station-based Pearson's correlation coefficients are shown in Figs. 11, 12, 13 and 14

relationship observed in winter and spring for the free troposphere Izaña station. Moreover, the decadal trend of the NAOI shows a significant decline in autumn over 1948–2014 (Table 5) which matched the decline in wind speed, while its positive but not significant decadal trend in winter might drive the weak decline or even increase of wind speed in this season. Furthermore, the recent negative but not significant tendency of the NAOI in winter and spring for 1989–2014, meaning suppressed trade-winds and more frequent cyclonic circulations might account for the decline of wind speed over the land–ocean environmental boundary and the strengthening of wind speed in the free troposphere at Izaña.

Lastly, the large-scale EA is complementary to the NAO on the wind speed variability in winter (also in autumn for 1948–2014), displaying negative and significant correlations over the northern half ocean region (Fig. 14); this relationship is negligible over land stations. Nevertheless, the major finding of the influence of EA on wind speed variability occur in summer, with a strong and significant correlation signal switching to positive for both land–ocean environments below the TWIL. Because the major influence of the EA on wind speed variability occurred in summer, the positive and significant decadal trend of the EAI is in summer (Table 5), which is associated with a reinforcement of trade-winds circulations, might partly explain the observed strengthening of north-easterly wind circulations in this season.

5 Discussion

This study filled a gap in the global map of wind speed trends compiled by McVicar et al. (2012), reporting multi-decadal variability of wind speed for the previously non-studied Canary Island archipelago and the surrounding Eastern North Atlantic Ocean, for 1948–2014. Under the influence of global warming, the poleward expansion of the Hadley circulation (Lu et al. 2007) and the stilling phenomenon (Roderick et al. 2007) mostly observed in mid-latitude regions (Vautard et al. 2010; McVicar et al. 2012), this region represents a ‘hot-spot’ because it is halfway between tropical and subtropical areas and is dominated by trade-winds associated with the subtropical high pressure belt (i.e., Azores anticyclone). The primary uniqueness of this research was to simultaneously analyse wind speed variability: (1) at the land–ocean interface, to prove differences between both environments; and (2) below–above the TWIL, to demonstrate a decoupling of wind speed variability and trends between atmospheric layers.

The reported wind speed trends from the 1980s onward (particularly for the common 1989–2014 extent), are in close agreement with recent findings observed in proximal subtropical regions (e.g., Azorin-Molina et al. 2014, 2016 for Spain and Portugal). For instance, a distinct seasonal trend pattern with a strengthening (late spring and summer), and weakening (winter–spring–autumn) of wind speed across both land and ocean surfaces below the TWIL was reported.

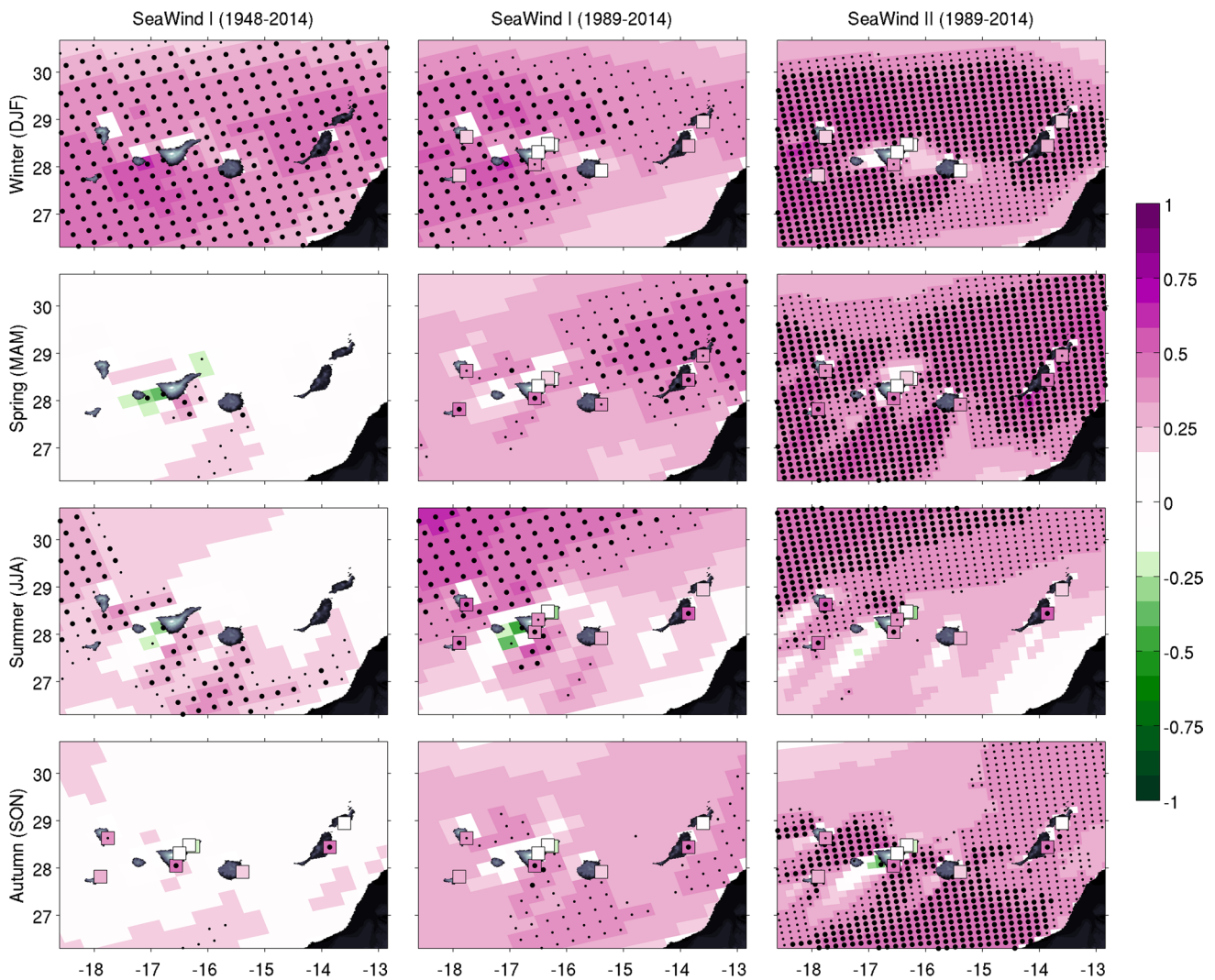


Fig. 12 Seasonal Pearson's correlation coefficient between wind speed anomalies and the TWI for SeaWind I (1948–2014 and 1989–2014), SeaWind II (1989–2014), and nine land-based observations

(for 1989–2014 only). The dots located in the centre of the grid-cells and squares (for observations) show the statistical significance of the trends at $p < 0.05$ (large dots) and $p < 0.10$ (small dots)

Even though few of the trends in Table 2 computed from the mean anomaly series are statistically significant for 1989–2014 (except for Izaña), the spatial distribution of the trends for every oceanic grid-cell and the land-based stations clearly demonstrated where winds have significantly increased (particularly in May and August) or decreased (particularly in April and September) during recent decades.

For the longer 1948–2014 period, SeaWind I reported significant declining trends for annual, seasonal and monthly time-scales. Despite the use of stable data assimilation systems in production of global reanalyses that in general produced fairly reliable records generally (Trenberth and Smith 2005), reanalysis products have shortcomings in capturing near-surface winds, as many surface layer processes controlling wind are not adequately represented (McVicar et al.

2008; Pryor et al. 2009; Vautard et al. 2010). SeaWind I hindcast showed a good performance when verified against in-situ buoy wind speed measurements over ocean (Menendez et al. 2014) and altimeter satellite observations (Fig. 2), yet it is possible that boundary and initial conditions from NCEP/NCAR reanalysed wind speed could have been positively biased (particularly during the 1950s and 1960s when limited ground-network and no satellite observations were used in the reanalysis modelling) and, therefore, resultant long-term 1948–2014 trends are negatively biased. Moreover, Menendez et al. (2014) concluded that SeaWind II (driven by ERA-Interim reanalysis) showed better performance in simulating oceanic wind fields across the entire Mediterranean Sea than SeaWind I (driven by NCEP/NCAR reanalysis). However, differences found by Menendez et al.

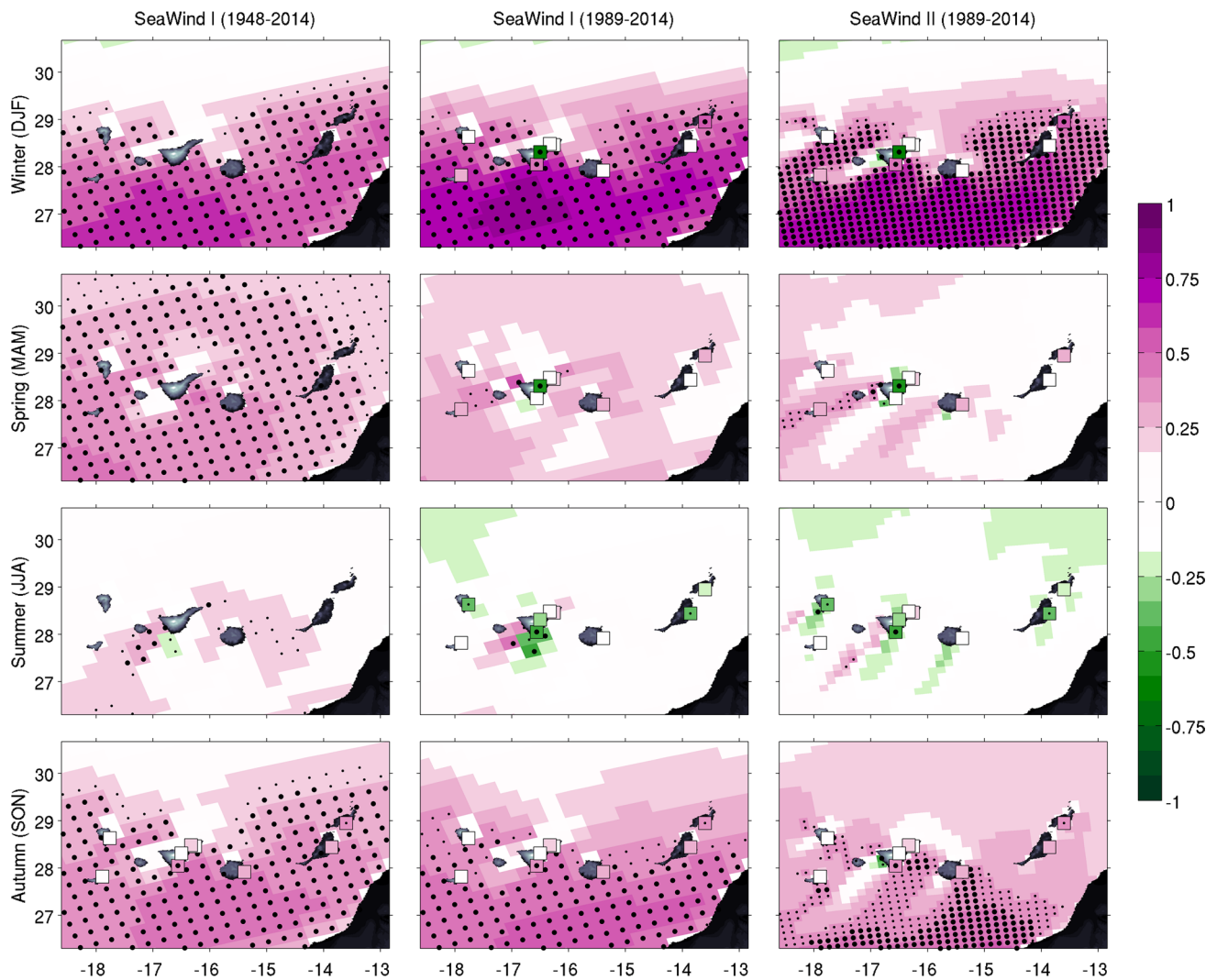


Fig. 13 The same as Fig. 12 but for the NAOI

(2014) were not large, as we also confirmed here when computing trends for the common 1989–2014 period. Therefore, the potential value of SeaWind I resided in spanning 67 years with high spatial resolution, as Sotillo et al. (2005) and Menendez et al. (2014) stated. Here we reported oceanic wind speed variability over the Eastern North Atlantic Ocean with higher horizontal resolutions (i.e., spacing of 30 and 15 km for SeaWindI and SeaWindII, respectively) than global wind speed trends presented by e.g., Wentz et al. (2007; 250 km) for 1987–2006, and Tokinaga and Xie (2011; 400 km) and Young et al. (2011; 200 km) for 1988–2008. In comparison to these studies which reported increasing global ocean wind speed trends, the SeaWind I and SeaWind II hindcast products reported annual declined wind speed trends around the Canary Islands for 1989–2014, with the abovementioned distinct seasonal trend pattern. In any case, the comparison of the sign, magnitude and statistical

significance of trends against previous studies is difficult to achieve because values are strongly sensitive to the start date and study period (McVicar et al. 2010; Troccoli et al. 2012).

This research revealed that across the land–ocean interface below the TWIL no statistically significant differences in the wind speed trends were found. This contrasts with the overall discrepancy in reported near-surface wind speed trends over land (i.e., negative trends; McVicar et al. 2012) and ocean (i.e., positive trends; Young et al. 2011), partly attributed to an increase in land-surface roughness (i.e., forest growth, land use changes and urbanization) as initially reported by Vautard et al. 2010, and recently confirmed by others (Bichet et al. 2012; Wever 2012; Wu et al. 2016). The lack of differences at the land–ocean interface below the TWIL may be due to the relative small area covered by the seven main islands comprising the Canary Islands archipelago (totalling 7446 km² of the 235,556 km² covered by

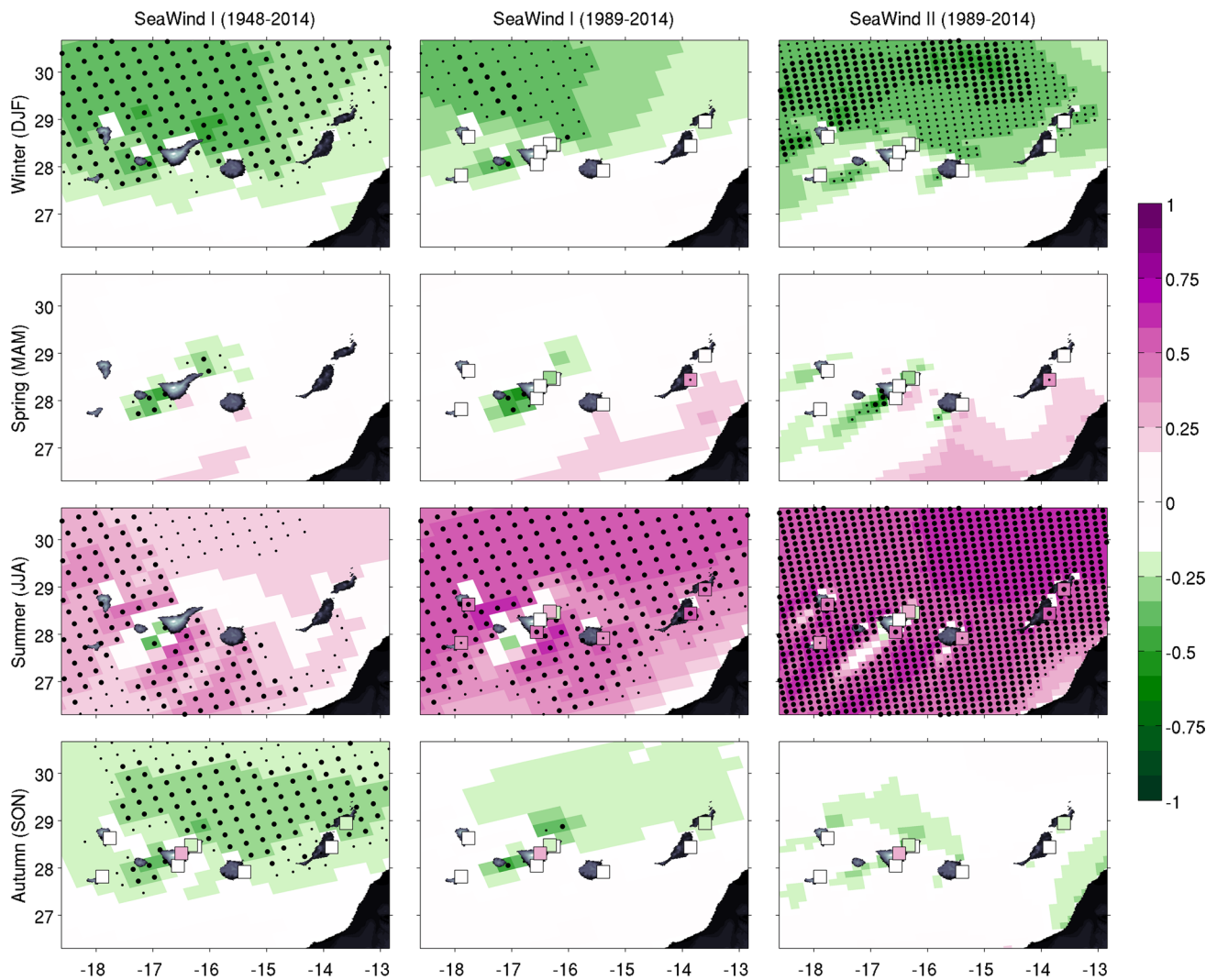


Fig. 14 The same as Fig. 12 but for the EAI

Table 5 Annual and seasonal trends of TWI, NAOI and EAI for 1948–2014 and for 1989–2014

Periods	TWI		NAOI		EAI	
	1948–2014	1989–2014	1948–2014	1989–2014	1948–2014	1989–2014
Annual	(0.095)	(0.134)	−0.064	(−0.370)	(0.175)	(0.256)
Winter (DJF)	0.050	0.053	0.054	−0.595	(0.235)	0.026
Spring (MAM)	(0.126)	0.066	−0.019	−0.263	(0.130)	0.238
Summer (JJA)	(0.117)	(0.234)	−0.104	(−0.715)	(0.169)	(0.410)
Autumn (SON)	(0.082)	0.169	(−0.191)	−0.015	(0.168)	(0.409)

Values are expressed as standardized sea level pressure difference. Statistically significant trends were defined as those where $p < 0.05$ (in bold and in parenthesis) and $p < 0.10$ (in bold)

both the SeaWind I and SeaWind II hindcast products), and most importantly, that wind speed observations were measured in well-exposed sites (i.e., airports) with few proximal environmental changes (e.g., urbanization) during last three decades.

However, it is noticeable that heterogeneity is a characteristic feature in the sign and magnitude of wind speed trends within the Canary Islands archipelago, with trend differences between land stations and when compared to the surrounding ocean because the role of local or regional

features (e.g., surface roughness; Wever 2012) against prevailing wind flows (Griffin et al. 2010). Therefore, even though the role of surface roughness (Vautard et al. 2010) on the global decline of wind speed over land when compared to the ocean surfaces has not been observed in this study, both simulations and observations revealed that local features play a key role in the reported trends (confirming results of Vautard et al. 2010; Griffin et al. 2010; Wever 2012). For example, high-spatial resolution hindcast products, particularly those downscaled from SeaWind II at 15-km horizontal grid-spacing, demonstrated the orographic effects of the Canary Islands on small-scale atmospheric processes in ocean winds (Chelton et al. 2004). In that sense, strengthening (i.e., “venturi effect” in the channels between the Canary Islands) and weakening (i.e., leeward side of the islands) of wind speed is clearly detected for the ocean close to the coastline, with direct impact on the reported trends. This confirms the results found by Menendez et al. (2014) for the Mediterranean Sea basin.

Concerning the wind speed variability at the high-elevation Izaña Atmospheric Observatory (above the TWIL), a decoupled wind speed tendency was found when compared to stations below the TWIL. The statistically significant opposite trends (and of greater magnitude) were detected when compared to those from both the ocean and land datasets below the TWIL. This decoupled behaviour is very likely driven by the different altitude-dependent atmospheric dynamics prevailing in both layers, with dominant north-easterly below the TWIL and north-westerly synoptic flows above the TWIL (Cuevas et al. 2013). The increasing wind speed trend of trade-winds in late spring (e.g., May) and summer (e.g., August) is likely linked with the increasing tendency towards positive phases experienced by the TWI and the EAI during summer, while above the TWIL (i.e., in the free troposphere), wind speed at Izaña is negatively and significantly correlated to the NAO, mainly in winter and spring, confirming Cuevas et al.’s (2013) findings. Therefore, the tendency of the NAOI towards a more negative phase (mainly in winter and spring) during 1989–2014 would result in a higher frequency of extratropical storms affecting subtropical latitudes, and thus in the increasing wind speed trend observed at Izaña. Moreover, the dominant positive tendency of wind speed observed in the mountainous Izaña station contrasts with results from McVicar et al. (2010), who showed that near-surface wind speeds are declining more rapidly at higher elevations than lower elevations as partly attributed to the observed increasing altitude of the tropopause (Santer et al. 2003). This reveals the limited knowledge about changes in wind speed in high-elevation (i.e., mountains) and high-altitude (i.e., atmosphere) regions (both within and above the boundary layer), and highlights the need for assessing wind variability at different

levels of the troposphere and latitudes across the globe (for both terrestrial and oceanic environments).

Lastly, to better assess trends/cycles and understand causes explaining changes in wind speed (e.g., the global stilling phenomenon; McVicar et al. 2012) near-future studies will focus on rescuing and homogenizing the longest observed wind speed time series, and to create more reliable datasets than previously available. The STILLING project (http://cordis.europa.eu/project/rcn/201175_en.html; last accessed 1 June 2017) is currently rescuing the longest wind speed series (starting prior to the 1960s) with the aim to provide a unique opportunity to statistically assess trends and cycles and atmospheric causes on longer time periods and with more reliable datasets than in previous studies. For the Canary Island archipelago, efforts are currently focused on rescuing, digitizing and homogenizing land wind speed observations since the mid-1910s (e.g., raw records in Izaña begins in 1916), and the STILLING project is open to collect and quality control historical wind speed observations (prior to the 1960s until now) from stations and Institutions around the world. Understanding past wind speed variability will help to better evaluate: (1) past significant declining trends showed in this study from the SeaWind I hindcast for 1948–2014; and (2) future projections of wind speed under a global warming scenario, in which Ma et al. (2016) has recently predicted an increase of near-surface trade-winds over the Eastern North Atlantic region for the twenty-first century.

6 Conclusion

Based on the analysis above, the following overall findings can be drawn:

1. SeaWind I revealed a widespread significant decline of near-surface oceanic wind speed for all time-scales for 1948–2014. For the common 1989–2014 period all SeaWind I, SeaWind II and the eight land stations below the trade-wind inversion layer showed no significant trends annually, but displayed a distinct seasonal pattern with a strengthening (late spring and summer; significant in May and August) and weakening (winter–spring–autumn; significant in April and September) of trade-winds. Above the trade-wind inversion layer in Izaña, free troposphere winds tended to significantly increase for almost all time-scales analysed.
2. Land observations resembled the same multi-decadal variability simulated over ocean, with a statistically significant agreement of the wind speed trends at the land–ocean interface below the trade-wind inversion layer. Above this inversion layer in Izaña, a decoupled variability and significant opposite trends of winds

compared to those observed in the boundary layer (i.e., below the trade-wind inversion layer) were found.

3. The TWI, NAOI, and EAI are significantly correlated with wind speed variability, denoting the key role played by changes in large-scale atmospheric circulation. The correlation patterns of these three atmospheric circulation indices showed a spatial and temporal complementarity in shaping wind speed trends: TWI (positive across the whole domain in spring, summer and autumn), NAOI (positive over the southern-half region in winter and autumn; negative in Izaña in winter and spring) and EAI (negative over the northern-half region in winter and autumn and positive across the whole domain in summer).

Acknowledgements C. A. -M. has received funding from the European Union's Horizon 2020 research and innovation programme under the Marie Skłodowska-Curie grant agreement No. 703733 (STILL-ING project). This research was also supported by the Research Projects: Swedish BECC, MERGE, VR (2014–5320), PCIN-2015-220, CGL2014-52135-C03-01 and *Red de variabilidad y cambio climático RECLIM* (CGL2014-517221-REDT). M.M is indebted to the Spanish Government for funding through the “Ramón y Cajal” program and supported by Grant PORTIO (BIA2015-70644-R). The authors wish to acknowledge the anonymous reviewers for their detailed and helpful comments to the original manuscript; the AEMET for the observed terrestrial wind speed data, particularly to Juan-José de Bustos (Izaña Atmospheric Observatory), and Dr. Thomas Cropper (University of Sheffield) for updating the Trade Wind Index dataset.

Open Access This article is distributed under the terms of the Creative Commons Attribution 4.0 International License (<http://creativecommons.org/licenses/by/4.0/>), which permits unrestricted use, distribution, and reproduction in any medium, provided you give appropriate credit to the original author(s) and the source, provide a link to the Creative Commons license, and indicate if changes were made.

References

- Aguilar E, Auer I, Brunet M, Peterson TC, Wieringa J (2003) Guidelines on climate metadata and homogenization. World Meteorol Organ. http://www.wmo.int/datastat/documents/WCDMP-53_1.pdf. Accessed 1 June 2017
- Alexandersson H (1986) A homogeneity test to precipitation data. *Int J Climatol* 6(6):661–675. doi: [10.1002/joc.3370060607](https://doi.org/10.1002/joc.3370060607)
- Azorin-Molina C, Vicente-Serrano SM, McVicar TR, Jerez S, Sanchez-Lorenzo A, López-Moreno JI, Revuelto J, Trigo RM, Lopez-Bustins JA, Espirito-Santo F (2014) Homogenization and assessment of observed near-surface wind speed trends over Spain and Portugal, 1961–2011. *J Clim* 27(10):3692–3712. doi: [10.1175/JCLI-D-13-00652.1](https://doi.org/10.1175/JCLI-D-13-00652.1)
- Azorin-Molina C, Guijarro JA, McVicar TR, Vicente-Serrano SM, Chen D, Jerez S, Espirito-Santo F (2016) Trends of daily peak wind gusts in Spain and Portugal, 1961–2014. *J Geophys Res Atmos* 121(3):1059–1078. doi: [10.1002/2015JD024485](https://doi.org/10.1002/2015JD024485)
- Barnston AG, Livezey RE (1987) Classification, seasonality and persistence of low-frequency atmospheric circulation patterns. *Mon Weather Rev* 115(6):1083–1126. doi: [10.1175/1520-0493\(1987\)115<1083:CSAPOL>2.0.CO;2](https://doi.org/10.1175/1520-0493(1987)115<1083:CSAPOL>2.0.CO;2)
- Bichet A, Wild M, Folini D, Schär C (2012) Causes for decadal variations of wind speed over land: sensitivity studies with a global climate model. *Geophys Res Lett* 39(11):L11701. doi: [10.1029/2012GL051685](https://doi.org/10.1029/2012GL051685)
- Carrillo J, Guerra JC, Cuevas E, Barrancos J (2016) Characterization of the marine boundary layer and the trade-wind inversion over the sub-tropical North Atlantic. *Bound Layer Meteorol* 158(2):311–330. doi: [10.1007/s10546-015-0081-1](https://doi.org/10.1007/s10546-015-0081-1)
- Chelton DB, Schlax MG, Freilich MH, Milliff RF (2004) Satellite radar measurements reveal short-scale features in the wind stress field over the world ocean. *Science* 303:978–983. doi: [10.1126/science.1091901](https://doi.org/10.1126/science.1091901)
- Clogg CC, Petkova E, Haritou A (1995) Statistical methods for comparing regression coefficients between models. *Am J Soc* 100(5):1261–1293. doi: [10.1086/230638](https://doi.org/10.1086/230638)
- Cropper TE, Hanna E (2014) An analysis of the climate of Macaronesia, 1865–2012. *Int J Climatol* 34(3):604–622. doi: [10.1002/joc.3710](https://doi.org/10.1002/joc.3710)
- Cuevas E, Gonzalez Y, Rodriguez S, Guerra JC, Gomez-Pelaez AJ, Alonso-Perez S, Bustos J, Milford C (2013) Assessment of atmospheric processes driving ozone variations in the sub-tropical North Atlantic free troposphere. *Atmos Chem Phys* 13(4):1973–1998. doi: [10.5194/acp-13-1973-2013](https://doi.org/10.5194/acp-13-1973-2013)
- Dadaser-Celik F, Cengiz E (2014) Wind speed trends over Turkey from 1975 to 2006. *Int J Climatol* 34(6):1913–1927. doi: [10.1002/joc.3810](https://doi.org/10.1002/joc.3810)
- Dunn RJH, Azorin-Molina C, Mears CA, Berrisford P, McVicar TR (2016) Surface winds. In *State of the climate 2015*. Bull Am Meteor Soc 97(8):S38–S40
- El Kenawy A, López-Moreno JI, Stepanek P, Vicente-Serrano SM (2013) An assessment of the role of homogenization protocol in the performance of daily temperature series and trends: application to northeastern Spain. *Int J Climatol* 33(1):87–108. doi: [10.1002/joc.3410](https://doi.org/10.1002/joc.3410)
- García-Santos G, Marzol MV, Aschan G (2004) Water dynamics in a laurel montane cloud forest in the Garajonay National Park (Canary Islands, Spain). *Hydrol Earth Syst Sci* 8(6):1065–1075. doi: [10.5194/hess-8-1065-2004](https://doi.org/10.5194/hess-8-1065-2004)
- Griffin BJ, Kohfeld KE, Cooper AB, Boenisch G (2010) The importance of location for describing typical and extreme wind speed behavior. *Geophys Res Lett* 37:L22804. doi: [10.1029/2010GL045052](https://doi.org/10.1029/2010GL045052)
- Jones PD, Jonsson T, Wheeler D (1997) Extension to the North Atlantic Oscillation using early instrumental pressure observations from Gibraltar and south-west Iceland. *Int J Climatol* 17(13):1433–1450. doi: [10.1002/\(SICI\)1097-0088\(19971115\)17:13<1433::AID-JOC203>3.0.CO;2-P](https://doi.org/10.1002/(SICI)1097-0088(19971115)17:13<1433::AID-JOC203>3.0.CO;2-P)
- Kalnay E et al (1996) The NCEP/NCAR 40-year reanalysis project. *Bull Am Meteor Soc* 77(3):437–471. doi: [10.1175/1520-0477\(1996\)077<0437:TNYRP>2.0.CO;2](https://doi.org/10.1175/1520-0477(1996)077<0437:TNYRP>2.0.CO;2)
- Kendall MG, Gibbons JD (1990) Rank correlation methods. Oxford University Press, p 272
- Kim J, Paik K (2015) Recent recovery of surface wind speed after decadal decrease: a focus on South Korea. *Clim Dyn* 45(5):1699–1712. doi: [10.1007/s00382-015-2546-9](https://doi.org/10.1007/s00382-015-2546-9)
- Lanzante JR (1996) Resistant, robust and non-parametric techniques for the analysis of climate data: theory and examples, including applications to historical radiosonde station data. *Int J Climatol* 16(11):1197–1226. doi: [10.1002/\(SICI\)1097-0088\(199611\)16:11<1197::AID-JOC89.3.0.CO;2-L](https://doi.org/10.1002/(SICI)1097-0088(199611)16:11<1197::AID-JOC89.3.0.CO;2-L)
- Livezey RE, Chen WY (1983) Statistical field significance and its determination by Monte Carlo techniques. *Mon Weather Rev* 111(1):46–59. doi: [10.1175/1520-0493\(1983\)111<0046:SFSASID>2.0.CO;2](https://doi.org/10.1175/1520-0493(1983)111<0046:SFSASID>2.0.CO;2)

- Lu J, Vecchi GA, Reichler T (2007) Expansion of the Hadley cell under global warming. *Geophys Res Lett* 34(6):L06805. doi:[10.1029/2006GL028443](https://doi.org/10.1029/2006GL028443)
- Ma J, Foltz GR, Soden BJ, Huang G, He J, Dong C (2016) Will surface winds weaken in response to global warming? *Environ Res Lett* 11:124012. doi:[10.1088/1748-9326/11/12/124012](https://doi.org/10.1088/1748-9326/11/12/124012)
- McVicar TR, Körner C (2013) On the use of elevation, altitude, and height in the ecological and climatological literature. *Oecologia* 171(2):335–337. doi:[10.1007/s00442-012-2416-7](https://doi.org/10.1007/s00442-012-2416-7)
- McVicar TR, Van Niel TG, Li LT, Roderick ML, Rayner DP, Ricciardulli L, Donohue RJ (2008) Wind speed climatology and trends for Australia, 1975–2006: capturing the stilling phenomenon and comparison with near-surface reanalysis output. *Geophys Res Lett* 35(20):L20403. doi:[10.1029/2008GL035627](https://doi.org/10.1029/2008GL035627)
- McVicar TR, Van Niel TG, Roderick ML, Li LT, Mo XG, Zimmermann NE, Schmatz DR (2010) Observational evidence from two mountainous regions that near-surface wind speeds are declining more rapidly at higher elevations than lower elevations: 1960–2006. *Geophys Res Lett* 37(6):L06402. doi:[10.1029/2009GL042255](https://doi.org/10.1029/2009GL042255)
- McVicar TR, Roderick ML, Donohue RJ, Li LT, Van Niel TG, Thomas A, Grieser J, Jhajharia D, Himri Y, Mahowald NM, Mescherskaya AV, Kruger AC, Rehman S, Dinpashoh Y (2012) Global review and synthesis of trends in observed terrestrial near-surface wind speeds: implications for evaporation. *J Hydrol* 416–417:182–205. doi:[10.1016/j.jhydrol.2011.10.024](https://doi.org/10.1016/j.jhydrol.2011.10.024)
- Menendez M, Garcia-Diez M, Fita L, Fernandez J, Mendez FJ, Gutierrez JM (2014) High-resolution sea wind hindcasts over the Mediterranean area. *Clim Dyn* 42(7):1857–1872. doi:[10.1007/s00382-013-1912-8](https://doi.org/10.1007/s00382-013-1912-8)
- Mestre O, Domonkos P, Picard F, Auer I et al (2013) HOMER: a homogenization software—methods and applications. *Q J Hung Meteorol Serv* 117(1):47–67
- Minola L, Azorin-Molina C, Chen D (2016) Homogenization and assessment of observed near-surface wind speed trends across Sweden, 1956–2013. *J Clim* 29(20):7397–7415. doi:[10.1175/JCLI-D-15-0636.1](https://doi.org/10.1175/JCLI-D-15-0636.1)
- Pinard JP (2007) Wind climate of the Whitehorse area. *Artic* 60(3):227–237
- Pryor SC, Barthelmie RJ, Young DT, Takle ES, Arritt RW, Flory D, Gutowski Jr. WJ, Nunes A, Roads J (2009) Wind speed trends over the contiguous United States. *J Geophys Res Atmos* 114(D14):D14105. doi:[10.1029/2008JD011416](https://doi.org/10.1029/2008JD011416)
- Roderick ML, Rotstain LD, Farquhar GD, Hobbins MT (2007) On the attribution of changing pan evaporation. *Geophys Res Lett* 34(17):L17403. doi:[10.1029/2007GL031166](https://doi.org/10.1029/2007GL031166)
- Santer BD, Wehner MF, Wigley TML, Sausen R, Meehl GA, Taylor KE, Ammann C, Arblaster J, Washington WM, Boyle JS, Brüggemann W (2003) Contributions of anthropogenic and natural forcing to recent tropopause height changes. *Science* 301:479–483. doi:[10.1126/science.1084123](https://doi.org/10.1126/science.1084123)
- Skamarock WC, Klemp JB, Dudhia J, Gill DO, Baker DM, Duda MG, Huang XY, Wang W, Powers JG (2008) A description of the advanced research WRF version 3. NCAR tech note NCAR/TN-475 + STR, p 125. doi:[10.5065/D68S4MVH](https://doi.org/10.5065/D68S4MVH). <http://nldr.library.ucar.edu/repository/collections/TECH-NOTE-000-000-000-855>. Accessed 1 June 2017
- Sotillo MG, Ratsimandresy AW, Carretero JC, Bentamy A, Valero F, Gonzalez-Rouco F (2005) A high-resolution 44-year atmospheric hindcast for the Mediterranean basin: contribution to the regional improvement of global reanalysis. *Clim Dyn* 25(2):219–236. doi:[10.1007/s00382-005-0030-7](https://doi.org/10.1007/s00382-005-0030-7)
- Stepanek P (2004) Anclim: software for time series analysis and homogenization. Department of Geography, Faculty of Natural Science, Masaryk University, 1.47 MB. <http://www.climahomeu/software-solution/anclim>. Accessed 1 June 2017
- Sterl A (2004) On the (in)homogeneity of reanalysis products. *J Clim* 17(19):3866–3873. doi:[10.1175/1520-0442\(2004\)017<3866:OTIORP>2.0.CO;2](https://doi.org/10.1175/1520-0442(2004)017<3866:OTIORP>2.0.CO;2)
- Tokinaga H, Xie SP (2011) Wave and anemometer-based sea-surface wind (WASWind) for climate change analysis. *J Clim* 24(1):267–285. doi:[10.1175/2010JCLI3789.1](https://doi.org/10.1175/2010JCLI3789.1)
- Trenberth KE, Smith L (2005) The mass of the atmosphere: a constraint on global analyses. *J Clim* 18(6):864–875. doi:[10.1175/JCLI-3299.1](https://doi.org/10.1175/JCLI-3299.1)
- Troccoli A, Muller K, Coppin P, Davy R, Russell C, Hirsch AL (2012) Long-term wind speed trends over Australia. *J Clim* 25(1):170–183. doi:[10.1175/2011JCLI4198.1](https://doi.org/10.1175/2011JCLI4198.1)
- Vautard R, Cattiaux J, Yiou P, Thépaut JN, Ciais P (2010) Northern Hemisphere atmospheric stilling partly attributed to an increase in surface roughness. *Nat Geosci* 3(11):756–761. doi:[10.1038/ngeo979](https://doi.org/10.1038/ngeo979)
- Venema VKC, Mestre O, Aguilar E, Auer I et al (2012) Benchmarking homogenization algorithms for monthly data. *Clim Past* 8(1):89–115. doi:[10.5194/cp-8-89-2012](https://doi.org/10.5194/cp-8-89-2012)
- von Storch H (1995) Misuses of statistical analysis in climate research. In: von Storch H, Navarra A (eds) *Analysis of climate variability: applications of statistical techniques*. Springer, pp 11–26
- Wentz FJ, Ricciardulli L, Hilburn K, Mears C (2007) How much more rain will global warming bring? *Science* 317(5835):233–235. doi:[10.1126/science.1140746](https://doi.org/10.1126/science.1140746)
- Wever N (2012) Quantifying trends in surface roughness and the effect on surface wind speed observations. *J Geophys Res Atmos* 117(D11):D11104. doi:[10.1029/2011JD017118](https://doi.org/10.1029/2011JD017118)
- Wilks DS (2006) On “field significance” and the false discovery rate. *J Appl Meteorol Climatol* 45(9):1181–1189. doi:[10.1175/JAM2404.1](https://doi.org/10.1175/JAM2404.1)
- Wu J, Zha J, Zhao D (2016) Estimating the impact of the changes in land use and cover on the surface wind speed over the East China Plain during the period 1980–2011. *Clim Dyn* 46(3):847–863. doi:[10.1007/s00382-015-2616-z](https://doi.org/10.1007/s00382-015-2616-z)
- Young IR, Zieger S, Babanin AV (2011) Global trends in wind speed and wave height. *Science* 332(6028):451–455. doi:[10.1126/science.1197219](https://doi.org/10.1126/science.1197219)